IPP-Report

IPP Max-Planck-Institut für Plasmaphysik

O. Gruber, K.H. Finken*, G. Fuchs*, J. Neuhauser, J.-M. Noterdaeme, B. Streibl, F. Wesner

* Forschungszentrum Jülich GmbH, D-52425 Jülich

Combined Application to the HGF Strategy Fund for the Funding Period 1999 - 2002 from the HGF Centres, IPP Garching and FZ Jülich, for "Optimized Stationary Tokamak Operation"

IPP 1/322
September 1999

O. Gruber, K.H. Finken*, G. Fuchs*, J. Neuhauser,
J.-M. Noterdaeme, B. Streibl, F. Wesner

* Forschungszentrum Jülich GmbH, D-52425 Jülich

Combined Application to the HGF Strategy Fund for the Funding Period 1999 - 2002 from the HGF Centres, IPP Garching and FZ Jülich, for "Optimized Stationary Tokamak Operation"

IPP 1/322
September 1999

Contents

Abstract

In the field of magnetic confinement in tokamaks the HGF research centres, IPP Garching and FZ Jülich, integrate their research programmes, resources and expertise with the aim of developing concepts for Optimized Stationary Tokamak Operation. These efforts are mainly concentrated on the issues of stationary operation and optimization of advanced scenarios with the goal of developing smaller fusion reactors.

This report contains the main physics and technological elements of the joint application of IPP Garching an FZ Jülich, submitted to the HGF Strategy Fund in spring of 1999. This application makes use of the specific properties of the two tokamaks: Current drive and profile control issues as well as effects of the plasma shape are treated on ASDEX Upgrade, while enhanced rotation frequencies of the dynamic ergodic divertor together with new diagnostics for observing magnetic field structures are to be used on TEXTOR-94.

1 INTRODUCTION

In the field of magnetic confinement in tokamaks the HGF research centres, IPP Garching and FZ Jülic, integrate their research programmes with the aim of developing concepts for Optimized Stationary Tokamak Operation. These activities are part of the long-term European research programme on thermonuclear fusion coordinated by EURATOM.

While the ITER design provides for the first time an integral solution for a burning fusion plasma machine, the efforts for concept improvements are mainly concentrated on the issues of stationary operation and further optimization with advanced scenarios towards smaller machines.

Stationary tokamak operation calls for maintenance of the plasma current, for which methods have to be developed to provide a high fraction of internally diffusion-driven 'bootstrap' and externally inductively and non-inductively driven currents. Partly use of the inductively driven currents limits the tokamak operation to a stationary, but still pulsed system, while the combination of bootstrap and externally non-inductive current drive offers the route towards steady-state operation. These plasma currents are not needed in a stellarator - a concept now being pursued in new devices to demonstrate its potential as an alternative to the tokamak. In both confinement concepts, tokamak and stellarator, sufficient heat and particle exhaust with adequate impurity control is also necessary for stationary operation. This calls for development of an integral solution comprising, for example, wall materials, plasma edge parameters, heat load distribution on large areas via impurity radiation, impurity screening, and helium exhaust. The poloidal divertor is the most developed concept, but external ergodization of the plasma edge, in particular with a rotating distortion field, is regarded as an important candidate for further optimization.

Recent experiments (see sec. 3.1.2) as well as theory show clear indications that an appropriate control of the current profile can lead to further confinement improvements resulting in internal transport barriers and the required bootstrap currents, giving hope that it might be possible to achieve ignition in a sizeably smaller device than in conventional regimes, and to operate a power reactor steady-state, at a high value of Q.

This joint application of IPP Garching and FZ Jülich is an important element of the strategy of the HGF centres in the field of magnetic fusion aiming at further optimization of the use of their resources and their expertise. Last year IPP Garching applied for a divertor for the W7-AS stellarator. This year's application pertains to advanced tokamak scenarios and stationary operation to be performed on the ASDEX Upgrade non-circular tokamak with poloidal divertor and elongated plasmas and the TEXTOR-94 circular tokamak with pumped limiter and dynamic ergodic divertor for stationary exhaust control.

The elements of the application helping to exploit the potential of optimized scenarios make use of the specific properties of the two tokamaks in addition to the different exhaust schemes: current drive and profile control issues and shape effects are treated on ASDEX Upgrade, while enhanced rotation frequencies of the dynamic ergodic divertor together with new diagnostics to observe magnetic field structures are used on TEXTOR-94.

2 OPTIMIZED STATIONARY TOKAMAK OPERATION

2.1 Concept Description

It is now generally recognized that operation with a high internally diffusion-driven bootstrap current fraction complemented by internal inductive and non-inductive current drive is the most promising option for an economically attractive stationary tokamak reactor. This has led to increasing attention being paid to such operating modes in the ITER programme, and to recognition of the associated physics problems as a central theme of tokamak research for the coming years. To realize "optimized" or "advanced" modes of operation, a tokamak has to achieve high values of β_N, with good energy confinement, and with MHD-stable current and pressure profiles compatible with the intrinsic characteristics of the bootstrap current, which is driven by pressure gradient. This combination is made self-consistent by the fact that reduced transport can lead to internal transport barriers displaying high pressure gradients. The second main item of stationary tokamak research is to achieve compability of this new concept of an "advanced tokamak" with stationary operation at high power and, simultaneously, with sufficient heat and particle exhaust.

Such plasma conditions have been realized with the "advanced" discharges on ASDEX Upgrade, JET, TORE-Supra, TFTR, DIII-D, and JT60-U, but - at the required values of β_N - only transiently, limited by MHD instabilities. Common to these regimes of operation is the flattening of the central current profile corresponding to a zero or even negative value of the central magnetic shear ($s = \frac{r}{q}\frac{dq}{dr}$, where q is the safety factor). There is increasing evidence that, in addition to magnetic shear stabilization of transport-driving fluctuations, a combination with $E \times B$ shear stabilization is required for the initiation of internal transport barriers (ITB) [1, 2]. On ASDEX Upgrade, various operating scenarios have been tested to achieve improved core confinement by modifying the current density profile by means of early additional heating in the current ramp to reduce current diffusion at low initial density ($\bar{n}_e < 3 \times 10^{19}\,\mathrm{m}^{-3}$). The two scenarios now described are the most promising ones:

1) ITBs with an H-mode edge in combination with a flat, but still monotonic, q-profile with $q_0 \geq 1$ are obtained, which offer stationary, inductively driven H-mode operation with increased performance in terms of confinement and β. Such q-profiles with $q_0 \approx 1 - 1.5$, resulting in l_i values above 0.8 at $q_{95} \geq 3$ together with broad pressure profiles ($p_o/ < p >< 3$), help to avoid ideal kink modes occurring at $\beta_N \geq 4l_i$ without wall stabilization. β_N values between 3 and 4 would be possible if the neoclassical tearing modes unstable under these conditions for $\beta_N > 2.2$ could be stabilized by active feedback control as described in (see sec. 2.3). Plasma shapes with higher elongation κ and triangularity δ than those now being used in ASDEX Upgrade ($\kappa < 1.8$, $\delta < 0.2$) should help by reducing Δ'.

2) ITBs with reversed shear and q_{min} values above 2 could only be transiently established in ASDEX Upgrade and other experiments both with plasma edge parameters comparable to L-mode and with an H-mode edge. Here, ITBs with L-mode edge are distinguished by steep pressure gradients in the barrier region, while discharges with improved core

confinement and H-mode edge exhibit more moderate gradients. These current profiles would offer the route to true steady-state, non-inductively driven tokamak operation combining improved performance and high bootstrap current fraction $f_{bs} = I_{bs}/I_p \propto \beta_N q_{95}\sqrt{A}$, at high $q_{95} \geq 4$ and $\beta_N \geq 4$. Low (m,n) neoclassical tearing modes are avoided by the reversed shear and $q_{min} > 2$, but ideal pressure-driven kink modes are already unstable at low β_N values owing to the broad j-profile with low l_i values. Besides profile optimization (broad pressure profiles) and plasma shaping (high triangularities), this instability can be stabilized by a nearby conducting wall, which acts as a perfect conductor for a rotating plasma. In ASDEX Upgrade the walls are fairly far away from the plasma, and their stabilizing influence is rather small. However, the passively stabilizing saddle loops (PSL) in ASDEX Upgrade, required for reducing the growth rate of the vertical instability, could be extended in the poloidal direction. Since for high pressure the mode is located mainly at the low-field side, a partial wall put here would have a highly stabilizing effect. $\beta_N \geq 4$ should be achievable, but the resistive wall modes possibly arising would again need active feedback control by coils creating toroidal n = 1 and 2 components at the wall.

To become a realistic option, both as an operating mode for ITER and for a power-producing reactor, attainment of such conditions has to be demonstrated over all longer time scales. This requirement has to be satisfied in stages, with different aspects linked to a progressively longer duration of the "advanced" operation mode. MHD modes have to be controlled over several energy confinement times and the questions relating to particle control, impurity transport, and divertor operation have to be realistically addressed. As pointed out by Moreau [3] and shown by in our time-dependent simulation calculations (see sec. 2.2), the mutual dependence of energy transport, current density (or q-profile), and pressure profiles leads to a complex dynamic evolution proceeding on the resistive skin time scale. (For example, a rising bootstrap current tends to drive the central current density down inductively.) In a non-circular cross-section device the situation is further aggravated by the strong link in the plasma centre between the current density and flux surface shape. Ultimately, also slow secular dynamics proceeding over many skin times and true steady-state operating conditions at zero loop voltage will also have to be studied.

ASDEX Upgrade has a high plasma-shaping capability, extensive experience with and knowledge of poloidal divertor operation, flexible and powerful heating (NBI, ICRH, ECRH), refuelling (main chamber and divertor gas puffing, high and low-field-side pellet injectors) and pumping (both turbomolecular and cryogenic) systems, and elaborate control and diagnostic systems. This makes ASDEX Upgrade particularly suited to investigating the physics of "advanced tokamak" scenarios. To meet these goals further, ASDEX Upgrade needs off-axis current drive capability, a modest upgrading of its power-supply system to extend the pulse lengths, and adaptation of the divertor to the optimal more highly triangular plasma shapes (see sec. 3.1.1). This will allow study of questions of divertor physics and particle/impurity control, MHD stability, and discharge dynamics on the time scale of a few skin-times, which are now the most urgent topics for establishing the credibility of "advanced" scenarios.

Correspondingly, the goal of the ASDEX Upgrade advanced tokamak programme is to

- test operating scenarios
  - freezing of the current profile during current ramp-up,

  - current profile control by current drive (up to 400 kA) (long pulse)
  - fuelling by pellets
- investigate the related core and edge physics (MHD stability, mode stabilization, and energy and particle transport) including edge-core coupling
- achieve stationary profiles compatible with the advanced tokamak concept (long pulse)
- develop divertor concepts for varying magnetic configurations
- develop the relevant diagnostics.

2.2 Off-axis Current Drive Requirements for Advanced Tokamak Scenarios in ASDEX Upgrade

One major goal of the advanced tokamak studies is to achieve stationary profiles and alignment of the reversed or flat shear profiles with the bootstrap curent driven by the pressure profile exhibiting an internal transport barrier. Besides flexible heating and particle fuelling systems, this also requires powerful current drive systems. The non-inductive current drive capabilities are presently limited to the predominantly on-axis NBCD using the nearly perpendicular NBI and will be extended to a partly more tangential off-axis NBCD system with up to 250 kA in the year 2000 (see 3.1.1).

To establish the current drive (CD) level and its radial distribution necessary for achieving stationary flat or even reversed shear profiles with $q_{min} > 1$ in the plasma core on ASDEX Upgrade, two sets of transport simulations have been performed with the 1-1/2D ASTRA code. In the first set, temperature and density profiles containing an internal transport barrier at about half plasma radius, $\rho = r/a \approx 0.5$, are imposed as barriers in the temperature or in both the temperature and the density, as observed in present advanced tokamak experiments, and just the current diffusion is simulated (fig. 1 for $I_p = 1$ MA). In the second set, the full transport equations are solved self-consistently, and the heating and CD time scenarios are optimized in the ramp-up and in the current flat-top phase to achieve and maintain shear-optimized profiles aligned with the pressure transport barrier.

In the simulations with fixed pressure profiles, the source for the off-axis CD is provided by nearly tangential NB injection with a broad distribution of the driven current centred around $\rho \approx 0.5$. As starting conditions a reversed current density profile ($I_p = 1$ MA) is used at t = 0. With flat central temperatures of 10 keV and with a driven current of 250 kA (delivered by 100 keV deuterium beams with a power of 5 MW) the current profile hardly changes any more after 5 s, becoming truly stationary after 15 s (constant E field across the radius). The bootstrap current is about 700 kA with a strong peak at the position of the high pressure gradient, while the necessary seed current on axis is provided by a small inductively driven ohmic current peaked at the highest plasma temperature. These numbers highlight two mandatory requirements for steady-state advanced tokamak operation, namely a high bootstrap current fraction to limit the CD power and – to create the bootstrap current – sufficient pressure gradients created by high confinement properties to limit the heating power required.

The results described are rather insensitive to other assumptions about the plasma parameters. For instance, using density profiles including also a transport barrier, but with the same line-averaged density, will not shift the position of the driven current to smaller

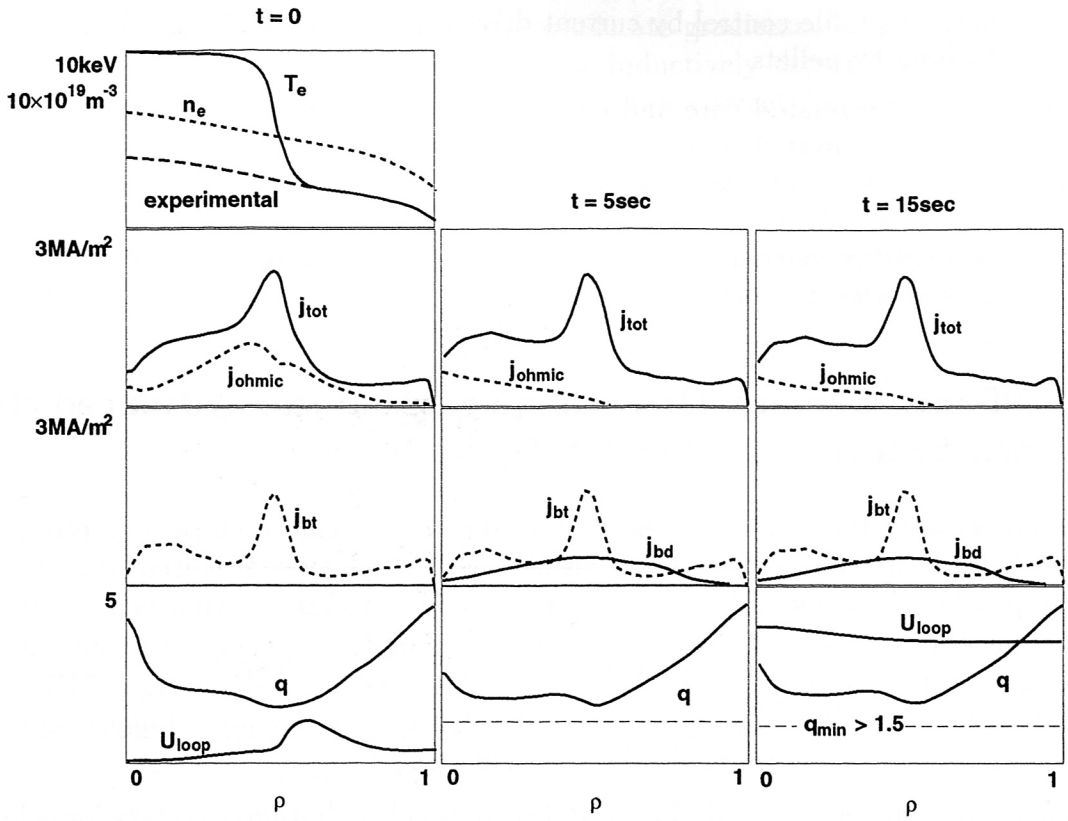

Figure 1: Modelling of neutral beam current drive with prescribed pressure profiles for 5 MW tangential NBI. The profiles in the left upper frame are kept constant in time.

radii. With this minimal off-axis CD of 250 kA the nearly flat q profile achieved in the plasma core is limited to $q_{min} \approx 1.5$. To achieve higher q_{min} values as proposed for scenario 2 in sec. 2.1, additional off-axis driven currents preferentially outside $\rho \approx 0.5$ are needed and could be provided by ICCD to get the necessary freedom for experimental investigations.

For the scenario optimization, the ASDEX Upgrade conditions for ramp rates of plasma and PF currents as well as of additional heating power schemes are used. The latter include early preheating with 1 MW ECRH during the current ramp-up to create reversed shear profiles, a stepped increase of the nearly perpendicular NBI power available up to 15 MW to heat the plasma centre and the proposed nearly tangential injection of up to 5 MW supplemented by 25 kA/MW ICCD for on/off-axis current drive to control the current profile. These time-dependent scenario calculations are done to prepare operating scenarios and confirm the results obtained with prescribed pressure profiles. To create the internal transport barrier, both the anomalous thermal conductivities for ions and electrons are switched off inside the reversed/flat shear region with $dq/d\psi \leq 0$ and only the neoclassical contributions are taken. The problem encountered is then given by the time evolution of the bootstrap current driven by the pressure increase due to the reduced transport, CD due to the perpendicular beams, the off-axis CD due to the tangential beams and the ICCD and the inductively driven ohmic current. Figure 2 shows various plasma parameters as functions of the absorbed ICR power. An optimization with respect to the radial location of the ICRH power deposition was made here. It is seen that a well-

pronounced reversed shear configuration with $q_{min} = 2$ at $\rho \approx 0.6$, $T_i(0) = 20\,\mathrm{keV}$, $\beta_N \approx 3$ can be obtained with the future heating and CD systems of ASDEX Upgrade.

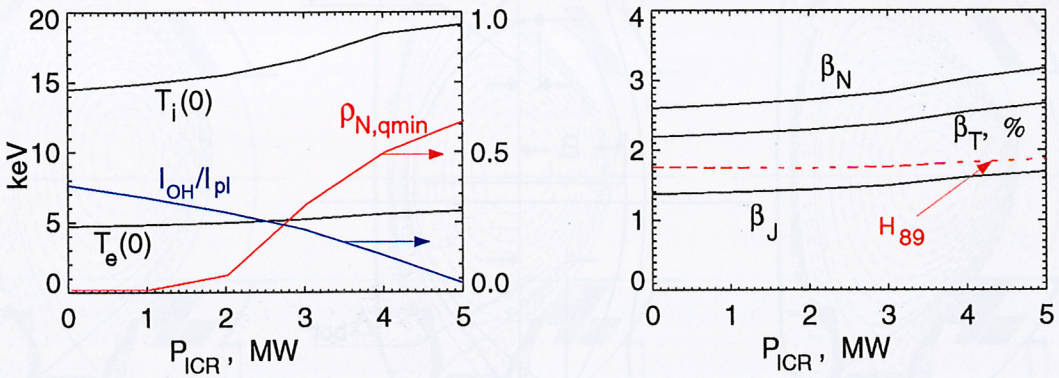

Figure 2: Core electron and ion temperatures, radius of the q_{min} position, and β-values as functions of ICCD power for $I_p = 1\,\mathrm{MA}$.

These results depend to some extent on the assumptions used since the physics of the transport barrier is not yet fully understood. Achievement of a stationary solution with a reversed shear/hot core region will therefore be a matter for exploration in our experiments. Our calculations demonstrate that an off-axis current drive of about 400 kA will allow relevant studies of such scenarios in ASDEX Upgrade.

2.3 Divertor Requirements for ASDEX Upgrade

The ASDEX Upgrade studies and other experiments on SOL and divertor physics seem to indicate that operation at high edge densities is a prerequisite for power exhaust with tolerable loads on the target plates. Specifically, under these conditions strong interlinks between the plasma edge and the bulk plasma, including the global confinement, have been observed. It is mandatory in this situation to widen the scope of the ASDEX Upgrade investigations to a more global view of the problems. Edge parameters influence core confinement in various ways. L-mode and H-mode confinement are discriminated by local edge parameters, core confinement is observed to depend on the edge pressure, and confinement enhancement by core density peaking is found in the H-mode regime with high radiated power fraction (CDH-mode). At the same time, edge parameters impose boundary conditions on divertor operation, e.g. detachment and density limit windows and power exhaust. Edge physics can therefore only be studied in the context of integrated solutions for the bulk, the edge, and the divertor; this is why ASDEX Upgrade has been progressively addressing the combined study of bulk, edge, and exhaust plasma physics.

It has been demonstrated in various tokamak experiments, including ASDEX Upgrade, that plasma shaping (especially higher triangularity) can strongly influence the confinement and ELM behaviour in the H-mode, and, correspondingly, the ITER-FDR design is based on a triangularity of $\delta_{top} = 0.2$ and $\delta_{bot} = 0.4$ (see fig. 3 for the definition of the triangularity δ used in this proposal). Later designs for a reduced-size ITER rely on even higher triangularities.

With the in-vessel components (ICRH antennae, PSL) used until summer 1998 in ASDEX

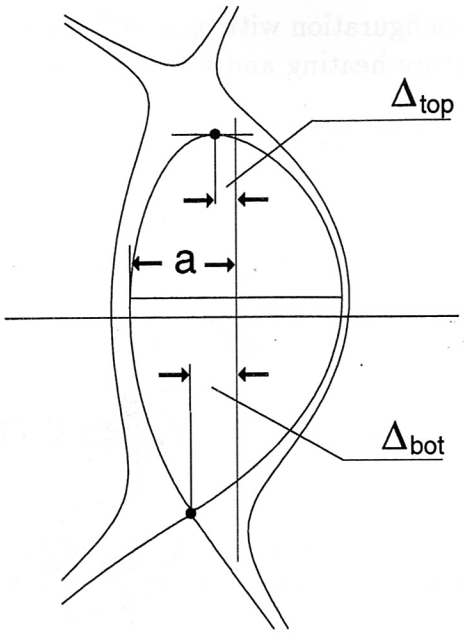

Figure 3: Sketch of plasma shapes defining the absolute triangularity Δ. The triangularity δ, which is used throughout this text, is normalized to the (horizontal) minor radius, $\delta = \Delta/a$.

Upgrade only equilibria with small triangularities of $\delta_{top} \leq 0.1$, $\delta_{bot} \leq 0.3$ (as shown in fig. 4a) could be investigated. Higher triangularities of $\delta_{top} \leq 0.4$, $\delta_{bot} \leq 0.5$ (fig. 4b and c) required modification of the ICRH antennae realized-autumn 1998.

With the poloidal field system (poloidal field coils outside toroidal field coils) and its power supplies given, the maximum possible triangularity is essentially determined by in-vessel components. The maximum radial plasma extent at the low-field side is determined by the position of the ion cyclotron antennae. Since further out the magnetic field ripple rapidly increases to intolerable values, this limitation would roughly persist even without an ion cyclotron launcher. On the high-field side the plasma is limited by the heat shield around the centre column. With these radial boundaries in the midplane given, the radial positions of the upper and lower X-points are obviously linked to the upper and lower triangularity, resp., according to definition. In parallel to the shift, there is some rotation of the separatrix structure around the X-points.

To maintain the leading properties of a single-null configuration, the top triangularity has to be kept smaller than the bottom triangularity. As a result, the average triangularity defined by $\delta_{av} = (\delta_{top} + \delta_{bot})/2$ may be varied for SN configurations between 0.15 and 0.45, hence by a factor of 3. This variation should permit a relevant experimental demonstration of the beneficial triangularity properties. The maximum average triangularity of $\delta_{av} \approx 0.45$ provides in addition the chance to access the favourable domain of Type II ELMs.

In a first stage, equilibria with higher triangularity can be run with the present divertor II and preparatory experiments regarding the effect of plasma shaping and different ramp-up scenarios will be carried out in this manner. For dedicated studies specifically addressing the compatibility of higher-triangularity equilibria with the divertor requirements, further modification of the divertor design is necessary, as described in sec. 5.

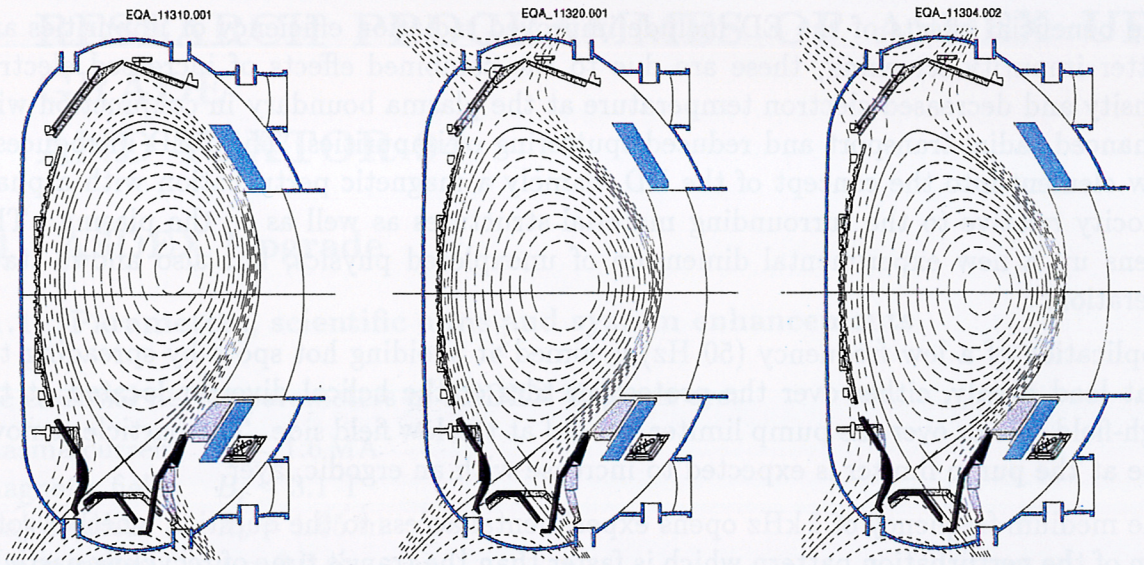

Figure 4: ASDEX Upgrade equilibria with the standard shape (a) and higher triangularity (b and c) with different β_p values. The shaded divertor structure is the present LYRA divertor, while the black contoured structure is the the proposed divertor IIb (see sec. 5).

2.4 Heat Exhaust and Particle Control Options of the Dynamic Ergodic Divertor (DED) of TEXTOR-94

One of the essential problems for the successful operation of a fusion burner is to arrange for the exhaust of heat and particles in such a way that the following requirements are met:

1) the materials and components of the inner wall are not overheated or unduly eroded
2) the pumping system and the geometrical arrangement of the wall components allow sufficient helium removal
3) only limited amounts of wall-released impurities, recycled helium, and injected impurities (for edge radiation cooling) are able to penetrate the boundary layer into the plasma core
4) the methods used to satisfy the above requirements are compatible with a high-energy confinement and a practical fuelling scheme.

Both to widen understanding of the physics involved in the exhaust issue and to explore possible alternative or complementing methods of exhausting particles and power, studies are also being undertaken on other concepts, in particular limiter concepts, the ergodic divertor, and the island divertor. An additional advantage of this programme strategy is the fact that (i) synergisms exist between different approaches and concepts and (ii) most methods and processes (such as diagnostics, wall treatment, modelling, heating) developed on one system can be transferred to the others.

The beneficial effects of the ED include improved radiation efficiency of impurities and better impurity screening; these are due to the combined effects of increased electron density and decreased electron temperature at the plasma boundary in conjunction with enhanced radial transport and reduced sputtering of impurities. The DED introduces a new element into the concept of the ED, namely a magnetic perturbation with a phase velocity relative to the surrounding material structures as well as to the plasma. This opens up a new experimental dimension of unexplored physics, but also allows static operation.

Application of a low frequency (50 Hz) is aimed at avoiding hot spots by spreading the heat load evenly, either over the protection tiles of the helical divertor located at the high-field side or over the pump limiter located at the low field side. The particle removal rate at the pump limiter is expected to increase with an ergodic layer.

The medium frequency of 1 kHz opens experimental access to the question whether rotation of the perturbation pattern which is faster than the transit time of recycling particles in the boundary layer will affect particle transport and, as a consequence, also the recycling process and screening efficiency.

In the highest frequency band of 1-10 kHz, the velocity of perturbation is then of the same order as the natural diamagnetic drift velocity of the plasma; here one can investigate whether the rotating field will induce an angular momentum in the plasma and whether the resulting torque will affect confinement and stability properties. A particularly interesting case may occur when the plasma rotation coincides with the rotation of the applied perturbation field. In this context, the DED addresses questions of plasma confinement and stability.

The high-frequency extension is part of this application, while the rest of the funding has already been approved.

A technical solution has been chosen to provide a wide range of experimental possibilities with limited investment, the aim being to explore the potential and limits of the DED as a means of influencing and controlling plasma-wall interaction. The benefit of the intended studies is seen to be an improved understanding of edge transport, island formation, effects of ergodicity etc. This may lead to incorporation of some features of the TEXTOR DED into other exhaust concepts and may also stimulate the search for novel concepts and technical solutions with development potential for a burning fusion plasma.

3 RESEARCH PROGRAMMES OF ASDEX UPGRADE AND TEXTOR-94

3.1 ASDEX Upgrade

3.1.1 Parameters, scientific aims and system enhancements

The essential device parameters of ASDEX Upgrade are:

plasma current	$I_p \leq 1.6\,\mathrm{MA}$
magnetic field	$B_t \leq 3.1$ T
major radius	$R_o = 1.65$ m
minor radius	a = 0.5 m
ellipticity	$\kappa \leq 1.8$
triangularity	$\delta_{top} \leq 0.4$; $\delta_{bot} \leq 0.5$
single-null divertor (double-null possible)	
NBI	two beamlines with $U = 65/100\,\mathrm{keV}$, $P_{NBI} = 20\,\mathrm{MW}$ (for D_2)
ICRH	4 antennae with $\nu = 30 \ldots 80$ MHz, $P_{ICRH} \leq 6\,\mathrm{MW}$
ECRH	4 gyrotrons (partly operational) with $\nu = 140$ GHz, $P_{ECRH} = 2\,\mathrm{MW}$
pumping	14 turbomolecular pumps: $S_{D_2} = 10\ \mathrm{m^3\ s^{-1}}$ in pump chamber; cryopump: $S_{D_2} = 100\ \mathrm{m^3\ s^{-1}}$

Target plates and near-plasma surfaces are covered with graphite (CFC at target tiles), and all surfaces are generally boronized.

The experimental programme of ASDEX Upgrade with its ITER-like cross-section is focused on

(i) edge and divertor physics in high-power, high-confinement regimes, with the aim of identifying and optimizing ways of safe power exhaust and particle control for next-generation divertor tokamaks,
(ii) confinement and performance related questions, where a close interaction between edge and core plasma behaviour has been realized, and
(ii) tokamak concept improvement (see sec. 2).

The similarity in cross-section with the other two European divertor tokamaks, Compass-D and JET, is important for determining size scalings for core, edge, and divertor physics. Additionally, the similarity to ITER in plasma shape, relative distance of the plasma to the poloidal field coils and the divertor and performance studies makes this device particularly suited to testing control strategies. Our efforts have led to a good understanding of and major achievements in both shape and the coupled plasma performance control for core, edge, and divertor parameters. These will now be extended to profile control.

In the edge and divertor physics programme the divertor I phase with "open" divertor configuration ended in 1996 using tungsten target plates, and the divertor II phase started in early summer 1997 with the "closed" LYRA version (including a roof baffle), which is rather similar to the present ITER reference design. It will be investigated without modifications till 2000, and the divertor configuration will then need to be adjusted to

more shaped plasmas with high triangularity ($\delta \leq 0.45$) as described in this application. The experiments on power loading, radiating scenarios, impurity production (low and high Z), and pumping processes (hydrogen, helium and impurities) using $P_h/R \leq 12\,\mathrm{MW/m}$ and power fluxes $\leq 8\,\mathrm{MW/m^2}$ are proceeing in close contact with a strong modelling effort including advanced 2D-codes such as B2-EIRENE. This work has reached a status of maturity which is providing the desired and timely input for the ITER divertor as an integral part of the international ITER physics R&D programme.

The ITER study offers a viable solution for the next step despite some remaining uncertainties, e.g. with respect to the achievement and quality of the desired high-confinement regime. To answer these questions, the main focus in the ASDEX Upgrade programme is progressively shifting towards core physics and tokamak concept improvement. In the core physics studies the physics close to regime transitions and operating limits have been especially investigated (transport, H-mode, scalings, MHD instabilities, and their stabilization). Here, one recent milestone was the successful demonstration of feedback stabilization of the beta-limiting neo-classical tearing modes by phase-coupled local ECRH/ECCD in the O-point of the unstable magnetic island. Reduction of the amplitude of the (3,2) mode and recovery of β have been achieved.

Milestones achieved in the area of tokamak concept improvements are:

- Flat and reversed shear profiles with $q(0) > 1$ and strongly reduced core transport were created by freezing the current profile with "early" heating (ECRH, ICRH, NBI) during current ramp-up, followed by stronger heating in the flat-top.
- A stationary H-mode scenario with internal transport barriers for ion and electron energies, particle, and momentum was maintained for 6 s, corresponding to 40 confinement times and several internal skin times ($H_{ITER-89P} = 2.4$, $\beta_N = 2$) with flat q-profile at $q(0) > 1$ (described in detail in sec 3.1.2).
- Attempts to increase β_N were limited by either (3,2) neo-classical modes in the case of flat q-profiles or (2,1) kink modes with reversed shear profile.

In the next few years these investigations will be continued with enhanced capabilities for higher-triangularity plasma shapes (improved MHD stability), the proposed off-axis current drive for current profile control (see below), and an adapted divertor. In long term stabilization of external kink modes with revesed shear profiles affords passive stabilization by a close first wall and active control of the possibly resulting resistive wall modes, while stabilization of neo-classical modes should be possible with ECRH/CD.

For the above-mentioned physics programme and the ASDEX Upgrade parameters, a heating power of about 20 MW (already in operation) is sufficient. Flexible use of this auxiliary power is provided by the availability of three different heating methods (NBI, ICRH, ECRH). However, for achieving stationary flat or reversed shear profiles (at $q_0 \geq 1$) an off-axis current drive capability of up to 400 kA is required at a plasma current of 1 MA (according to sec. 2.2).

In principle, ASDEX Upgrade can use the RF systems for current drive. The ICRH system has coupled its nominal power of 6 MW for plasma heating after the installation of four 3 db couplers in 1998, while current drive using mode conversion (up to 150 kA off-axis) is part of this applicaton and should be available in 1998. First estimates show that ECCD for ASDEX Upgrade conditions might allow a flexible current drive scheme,

but with an efficiency of only 14 kA/MW (off-axis). The RF systems now available would therefore not be sufficient to deliver the required additional current drive of 250 kA. RF current drive of 150 kA would require an extension of the ECRH system to more than 8 MW. This would call for the use of not yet available 1 MW steady-state gyrotrons, large additional installations, and high costs.

NBCD has a rather high current drive efficiency, and some complements to ICCD, namely
- driving toroidal rotation for mode stabilization,
- no restrictions on operation with respect to coupling requirements.

NBCD will therefore be used as the main tool for off-axis current drive on ASDEX Upgrade, while the off-axis ICRF current drive of up to 150 kA will be used for flexibility and additional requirements based on scenario considerations (sec. 2.2).

According to this programme the following priority support actions have been approved by EURATOM.

Turning the present nearly perpendicular NB injector 2 (100 keV D^0) in a more tangential] injection direction with all 4 sources still available (2 sources for CD of about 250 kA and 2 for heating) results in an only slightly off-axis peaked current drive profile. As the deposition maximum is required to be at $\rho_{pol} \sim 0.5$, the NBI box has to be moved further away from the tokamak. With this geometry, two heating sources still inject radially, and the power using exclusively for plasma heating is 15 MW. 5 MW is injected tangentially and therefore provides both current drive and plasma heating. At least one year is needed for turning the injector, which is envisaged for 2000/2001.

Extension of the flat-top pulse length to 10 s (corresponding to a few skin times) requires exploitation of the full flywheel energy of the different generators at IPP by compensating the reactive power of the thyristor converters with capacitors (by up to 120 MV Ar in 2000). A proper mix of additional heating units, needed only during the flat-top phase, and power supplies for the PF field coils will then permit balancing of the apparent power during the ramp-up and flat-top phases.

3.1.2 Stationary H-mode with Internal Transport Barrier on ASDEX Upgrade

A stationary regime of operation has been found which shows improved core confinement of both electrons and ions caused by an internal transport barrier (ITB) in combination with an H-mode edge [4]. In fig. 5, the main plasma parameters of such a discharge are illustrated. During the current ramp of 0.8 MA/s moderate neutral beam heating of 2.5 MW is applied. At t = 1 s the X-point is formed and the L-H-transition occurs. After the current flat top is reached, the NBI power is raised to 5 MW and the line-averaged density is kept at $4 \times 10^{19}\,m^{-3}$.

While the electron and ion temperatures increase at the same rate during the current ramp at a heating power of 2.5 MW, T_i reaches almost twice the value of T_e when the heating power is doubled. Central values of $T_i = 10$ keV and $T_e = 6.5$ keV, $H_{ITER89-P} = 2.4$, and $\beta_N = 2$ are maintained for 6 s, limited only by the programmed duration of the NBI. This corresponds to 40 confinement times or 2.5 resistive time scales for internal current redistribution, which here is the time taken by a current perturbation to diffuse over half

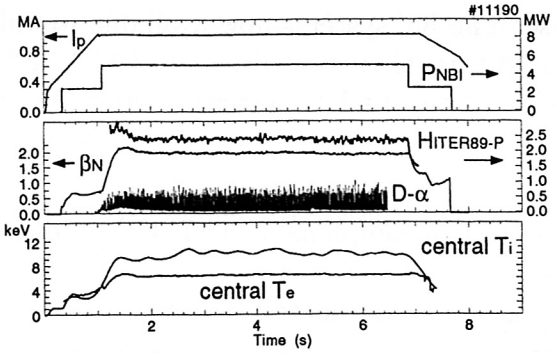

Figure 5: Time evolution of plasma current (I_p), neutral beam heating power (P_{NBI}), H-factor ($H_{ITER89-P}$), normalized beta (β_N), divertor D radiation, and central electron and ion temperatures ($T_{e,i}$) for a stationary discharge with ITB and H-mode edge. The toroidal magnetic field is $B_{tor} = 2.5T$.

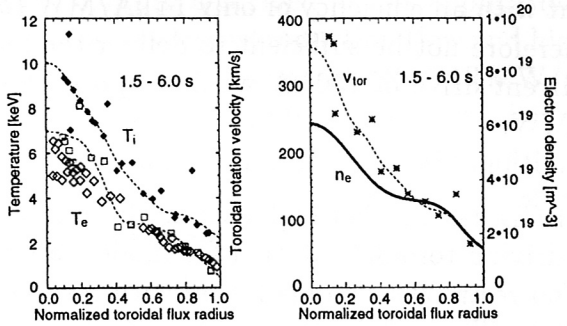

Figure 6: Radial profiles of ion and electron temperatures, electron density, toroidal rotation velocity (v_{tor}) of the discharge presented in fig. 5. The profiles are the average from 1.5 to 6 s covering most of the 5 MW heating phase.

of the minor radius. The perturbation was assumed to be located inside the half-radius region and to conserve the total plasma flux. The 8-channel motional Stark effect (MSE) polarimeter data show that the current profile remains stationary shortly after the full neutral-beam power is applied. In addition, the measured loop voltage is also stationary within 10%. These discharges resulted in the highest value of $n_{D,0} \times T_{i,0} \times \tau_E$ (7.5×10^{19} keV s m^{-3} for 6 s and 8×10^{19} keV s m^{-3} for 1 s) so far observed on ASDEX Upgrade.

The profiles of the plasma temperature, density, and toroidal rotation velocity (see fig. 6) show, in addition to the H-mode pedestal, a step starting at $\rho_{tor} = 0.6$ which is less pronounced in relation to ASDEX Upgrade transport barriers with L-mode edge, . The density peaking is $n_{e,0}/\overline{n}_e = 1.5$. Energy transport has been analyzed with the 1-1/2-D ASTRA code. In the central regions of the plasma the ion thermal conductivity drops to neoclassical values, but also the electron thermal conductivity is at a low level, indicating that the transport reduction is not limited to the ions, as seen in fig. 7.

The resulting q-profile is flat in the centre with $q \approx 1$ inside $\rho_{tor} = 0.2$, which is consistent with the location of the observed (1,1) fishbone mode derived from the SXR oscillations. The composition of the current density profile from ASTRA, which solves the current diffusion equation by means to the experimental temperature and Z_{eff} evolution is illustrated in fig. 7b. The total current profile is flat in the centre, but still monotonic, which is supported by the bootstrap current having its maximum close to the centre owing to a smaller pressure gradient as compared with internal transport barriers with L-mode edge. These stationary discharges with ITB are mainly inductively driven ($U_{loop} = 0.15$ V) and exhibit on-axis peaked ohmic, bootstrap, and beam ion driven currents. The moderate bootstrap current fraction of 25% of I_p is due to the $\beta_N = 2.2$ limit for this scenario, which, however, offers a potential for long-pulse, stationary operation with high central $n\tau T$ values and good performance.

When increasing the beam power, β_N is limited by the occurrence of (3,2) neoclassical

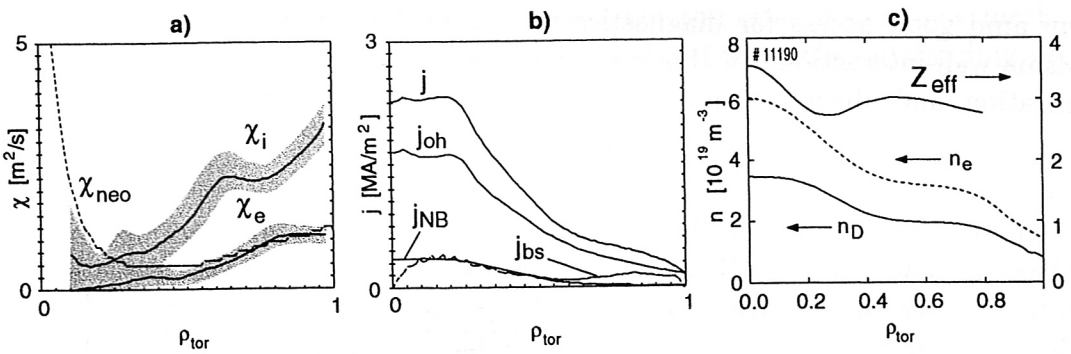

Figure 7: Radial profiles from ASTRA analysis for stationary ITB discharge with H-mode edge (at 2.5 s of # 11190). a) Ion and electron thermal conductivities. b) Composition of current profile. Shown are the total current density and the contributions of ohmic current (oh), neutral-beam current drive (NB), and bootstrap current (bs).

tearing modes, the onset of which is always preceded by a fishbone. Considering that sawteeth are not present, the second harmonic of a (1,1) fishbone acts as a seed island for the initiation of (3,2) neoclassical tearing modes [5]. The resulting β-limit is close to $\beta_N = 2.2$. At 6.25 MW of NBI, $\beta_N = 2.2$ could still be maintained for a duration of 1 s, after which a (3,2) mode occurred owng to the proximity to the β-limit. With further increased heating power (up to 10 MW), transient phases with higher $\beta_N \to 3$ and $H_{89P} \to 3$ are observed which are terminated by neoclassical tearing modes. Owing to the low density, the (3,2) modes were usually followed by (2,1) modes which ultimately lock.

3.2 Parameters and Scientific Aims of TEXTOR-94

The essential device parameters of TEXTOR-94 are:

plasma current	$I_p \leq 800$ kA
magnetic field	$B_t \leq 2.8$ T
major radius	R = 1.75 m
minor radius	a = 0.5 m (circular plasma)
NBI	2 beamlines (co, ctr) with 55 keV, $P_{NB} = 5$ MW
ICRH	2 antennae, $P_{ICRH} = 4$ MW
ECRH	$P_{ECRH} = 0.5$ MW at the end of 1999, later 2 MW FE planned
pumped limiter	ALT-II toroidal belt limiter, 8 movable blades, turbomolecular pumps
other limiters	a) poloidal limiters, movable during discharge
	b) test limiters, exchangeable through lock system
	c) inner bumper limiter, used as divertor plate for DED

The main limiter material is graphite; the poloidal limiters or the test limiters can be partly replaced by other materials (e.g. tungsten).

The baking capacity of TEXTOR-94 is an essential element of wall conditioning: the liner can be heated up to 500° C; baking of the vessel up to 300° C is possible. This feature and also other elements of the TEXTOR design, e.g. exchangeable liner, flexible limiter

system amd good access for diagnostics to plasma boundary, are optimized for study of plasma-wall-interaction. In this respect pioneering of coatings such as carbonization, boronization, and siliconization has been one of the outstanding results of TEXTOR.

Under carbonized and boronized conditions high-density operation became possible, allowing us to study detached ohmic plasmas – a plasma state with a cold radiating mantle and reduced minor radius of the hot plasma core (= detached from the limiter). At high heating power with NBI and ICRH on TEXTOR it has been demonstrated that up to 90% of the total heating power can be exhausted by line radiation with the help of injected noble gases (neon, argon) and feedback control of the radiation level under quasi-stationary conditions. This is possible, even at high densities, without detachment. Thus, the pumped limiter ALT-II is still operative.

With the pumped limiter ALT-II efficient He exhaust has been demonstrated, yielding a ratio of the effective He-confinement time τ^*_{He} and the energy confinement τ_E of $\tau^*_{He}/\tau_E = 10$. Rather good values have also been obtained at high densities and a high radiation level.

A significant improvement of energy confinement under high-power, high-radiation conditions has been found. Compared with the confinement scaling of H-mode plasmas, these discharges show a confinement as good as or even better than the ELM-free H-mode. The improvement increases linearly with density – the same scaling as the linear ohmic confinement regime. The regime found on TEXTOR-94 has been named "RI-mode". It is linked with peak density profiles. Quasi-stationary conditions can be achieved, as is demonstrated with, for example, an RI-mode discharge duration of 160 energy confinement times, limited only by the flux swing of the transformer.

Motivation for further investigation of the RI-mode is the fact that it simultaneously combines many features, required for a reactor: power load on large areas via radiation, operation at high densities above the Greenwald density, quasi-steady-state, and good energy confinement. The RI-mode is thus one outstanding field of research on TEXTOR-94. Related experiments on other machines (e.g. JET) are also planned, as well as a comparison with other improved confinement modes such as H-mode or a combination of edge H-mode barriers and RI-mode (e.g. similar to CDH-mode on ASDEX Upgrade).

The first decade of research on TEXTOR demonstrated that it is not recommendable to study plasma-wall interaction alone, isolated from core plasma physics. The close interrelation of edge physics and core physics is manifested clearly with, for example, the RI-mode. Therefore, with the foundation of the Trilateral Euregio Cluster (TEC) of the EURATOM associations, FZ-Jülich, ERM/KMS Brussels, and FOM Nieuwegein, in 1996 the expertise and the resources for investigating all plasma regions – wall, edge, and core – became available and a joint research programme on TEXTOR-94 under the title "development of an integral concept for energy and particle exhaust in fusion devices" had been started.

The research programme is now concentrated on the main topics of plasma-wall interaction, energy confinement, impurity transport, MHD, numerical modelling, and the development of new techniques.

Further optimization of the integral concept is being pursued, on the one hand, by improving our understanding of, for example, sawteeth and other MHD phenomena, impurity

transport, and erosion and deposition processes. On the other hand, new methods of influencing and controlling transport will be explored. Of these the outstanding projects are

a) the dynamic ergodic divertor (DED) and

b) well-localized electron cyclotron heating for generating internal transport barriers.

In the year 2000 the DED will be installed at the high-field side of TEXTOR-94. Magnetic perturbation coils will ergodize the plasma edge region. A near field (laminar zone) will divert the plasma to the inner bumper limiter. By appropriate phasing of the coils the distorting field is rotated in the poloidal direction. In the basic version the rotation frequency can be varied between 0 and 1 kHz. This already provides the means to distribute the power load on large areas of the inner bumper limiter and to optimize (minimize) the amount of injected impurities to obtain a high radiation level.

With the high-frequency operation up to 10 kHz (this application) a new field of research will be opened where, for example, torque transfer might generate sheared rotation and lead to the formation of transport barriers at the edge. Furthermore, it is speculated that the DED operation might improve the He exhaust capability of the pumped limiter ALT-II, which under the present RI-mode conditions is too low, after the limiter tiles have been made thicker.

The DED is thus envisaged as an important element of the TEC research programme towards an integral solution and might turn out to become a pioneering experiment for a novel concept of active transport control at the plasma boundary.

4 SUB-PROJECT 1: MODIFICATION OF THE ICRH SYSTEM ON ASDEX UPGRADE FOR OFF-AXIS CURRENT DRIVE UP TO 150 kA AND CURRENT DENSITY PROFILE CONTROL

Scientists responsible: F. Wesner, J.-M. Noterdaeme (IPP Garching)
For Ion Cyclotron Resonance Heating (ICRH) or Ion Cyclotron Current Drive (ICCD) electromagnetic waves with frequencies in the range of the cyclotron frequencies of plasma ions are launched into the plasma, transferring their energy to the plasma particles. Depending on the applied frequency and wave spectrum, the magnetic field, and the plasma particle mixture, heating of either ions or electrons can be achieved, or a toroidal plasma current can be driven. The power deposition area in the plasma can also be chosen, thus influencing the temperature and current profiles. Especially the flat or hollow plasma current profiles required for the optimized tokamak experiments with internal transport barriers can be achieved by driving positive off-axis or negative on-axis counter currents.

On ASDEX Upgrade so far only plasma heating using symmetric wave spectra has been applied. Asymmetric wave spectra needed for current drive call for waves propagating in one toroidal direction. Such waves cannot be launched with the present RF system. The required modifications and the experimental investigation of the current drive characteristics, as described in the following, are the subject of this application.

4.1 Physics of Current Drive with ICRF

4.1.1 ICCD schemes available

Current drive with an ICRF system can provide part of the current for a driven steady-state tokamak and, when an ITB is present, allows adjustment of the current profile as required to maintain the ITB. The current profile can be influenced indirectly and directly with ICRF: indirectly, by using ICRF heating (with a symmetric antenna spectrum) through the effect of the narrow power deposition on the bootsstrap current; directly, with an asymmetric antenna spectrum in three ways:

With the ICRF waves coupled to the ions, the resonance condition is

$$\omega - k_{//} v_{//i} = \omega_{ci},$$

and the ions with $k_{//} v_{//i} > 0$ are preferentially heated on one side of the resonance layer $\omega > \omega_{ci}$, while ions with $k_{//} v_{//i} < 0$ are heated on the other side of the resonance layer, where $\omega < \omega_{ci}$. This means that, with an asymmetric $k_{//}$ spectrum, a differential current can be driven near the resonance layer, resulting in flattening or steepening of the current profile there. This method has been effectively used on JET, for example, to influence the sawteeth [6].

With the wave directly coupled to the electrons, the resonance conditions for the electrons is

$$\omega - k_{//} v_{//e} = 0.$$

Here one has to distinguish between two ways.
a) When there is no resonant absorption on ions (which would otherwise dominate), and the fast wave propagates freely, the power is absorbed by the electrons near the centre. Depending on the direction of the asymmetry of the spectrum, the driven current adds to or subtracts from the existing current in the centre, resulting in steepening or flattening of the current profile there. For ITB experiments, flattening of the current profile is more advantageous. Experiments with FWCD were performed on D-III-D [7, 8, 9], TFTR [10], and Tore Supra [11]. For further reference we call this method Fast Wave Current Drive (FWCD).
b) With two ion species and the appropriate choice of frequency, magnetic field, and relative concentration of the ion species, a set of ion-ion hybrid and cut-off layers appears in the plasma. At the ion-ion hybrid layer, the fast wave is transformed (mode-converted) to a short wavelength ion Bernstein wave, which quickly damps on the electrons. We refer further to this as Mode Conversion Current Drive (MCCD). The location of the ion-ion hybrid layer can be positioned at will (with some restrictions) in the plasma, providing a way to drive current very locally, also outside the centre. Experiments in this direction were performed in TFTR [12].

The most promising methods of controlling the current profile in the ITB regime are FWCD and even more, MCCD because of the possibility of choosing the position of the driven current and the better absorption in this regime. Whereas current drive using ICRF has been investigated in several machines worldwide, ASDEX Upgrade would be the first to use this tool to optimize the ITB regime.

4.1.2 Theoretical background and estimates

Computer codes to calculate the power deposition profile in the ICRF regime exist at different levels of sophistication: from codes in slab geometry with simplifying assumptions to codes taking the full toroidal geometry into account under more realistic plasma conditions. The codes have been cross-checked worldwide [13], and with experiments. The situation is not so advanced with respect to theoretical estimates of current drive. Usually, calculated power deposition profiles are combined with a simple semi-analytic formula [14] that estimates the ratio of the driven current to the power absorbed on the electrons, in order to obtain the total driven current and its profile. This is only partially satisfatory in that the approximate formula was derived under conditions which are not always applicable. In order to improve on this situation a three-year cooperation with Kharkov University, funded by the WTZ, was initiated in 1997 and is expected to provide reliable estimates for the ICRF scenarios envisaged in ASDEX Upgrade in time for the start of the experiments. This will also allow further optimization of the ICRF parameters for the planned experiments to maximize, the driven current at the location chosen. For ASDEX Upgrade, the values were presently estimated on the basis of the above-mentioned combination of power deposition profiles and semi-analytic calculations,

but mainly from scaling of the values obtained on other experiments in the following way: The current drive efficiency is defined as

$$\eta = nRI/P,$$

where n is the average plasma density, R the major radius of the tokamak, I the driven current, and P the current drive power. Several experiments (D-III-D, Tore Supra) have shown [15] that in the ion cyclotron frequency range the current drive efficiency is proportional to the temperature:

$$\eta = (0.7 - 1) \cdot 10^{17} A/Wm^2 * T_e.$$

Combining the two formulas above allows an estimate of the total driven current in ASDEX Upgrade, for given radius, density, and temperature.

For FWCD, one has to avoid ion cyclotron resonances, where the ion absorption would compete with the electron absorption and would dominate. For 30 MHz (the lowest frequency of the ASDEX Upgrade generators), the H cyclotron resonance can be positioned on the low-field outside of the plasma, and the D cyclotron resonance on the high-field side outside the plasma near 2.7 T. The calculated power deposition profile, which to first order can be equated to the driven current profile, indicates that half the driven current is located within 30% of the minor radius. The total estimated current, based on extrapolation from the experiments and with reasonable assumptions concerning the fraction coupled to the electrons and the directivity of the antenna spectrum, is 100 kA for 4 MW at $n = 5 \times 10^{19}\,\mathrm{m}^{-3}$ and $T_e = 4\,\mathrm{keV}$.

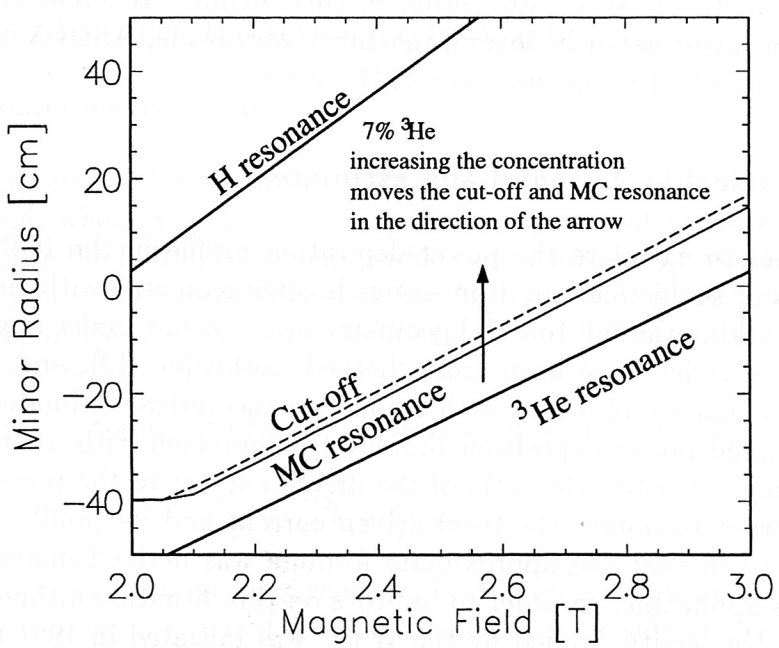

Figure 8: Position of the mode conversion layer for 7% ^{3}He in H.

For MCCD, several combinations of ions, their concentration, magnetic field, and generator frequency can be chosen. Figure 8 shows for a H plasma, with 7% ^{3}He the position of

the mode conversion layer (i.e. roughly the position of the driven current) as a function of the magnetic field at 30 MHz. The driven current can be positionned close to r/a = 0.4 with B = 2.5 T. Under these conditions the estimated current is 150 kA for 4 MW. For D as majority, at the same central magnetic field (2.5 T), the position of the driven current is at a higher r/a value.

4.1.3 Pilot experiments on ASDEX Upgrade

Because current drive requires an asymmetric (directional) antenna spectrum, and the present system configuration only permits a symmetric spectrum, the technical changes described below have to be implemented first to allow an asymmetric antenna spectrum and actually perform current drive experiments. However, pilot experiments which can answer two fundamental questions can and have been performed with a symmetric spectrum.

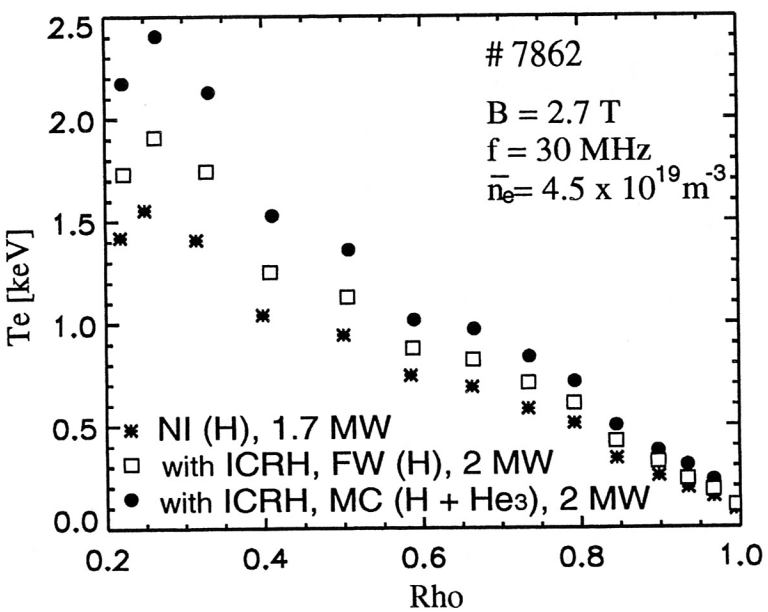

Figure 9: Electron temperature profile versus normalized plasma radius with and without direct electron heating.

1. Tests using different heating scenarios showed that coupling to the electrons is possible:
a) Under the conditions envisaged for FWCD (no ion resonance in the plasma), it was shown that central heating of the electrons, at the same time avoiding resonant ion heating, is possible (fig. 9).
b) Similarly, under MCCD conditions (two ion species), coupling to the electrons off-axis was measured. The heating of the electrons was more efficient than in the case of FW electron heating. Both in the combinations ^{3}He in H, and ^{3}He in D, the power deposition profile on the electrons was measured, see fig. 10 [16]. It was also shown that, by vary-

ing the ^{3}He concentration, the position of the power deposition moves across the plasma radius, thereby strongly influencing the sawtooth behaviour [17]. This provides a first indication that it should be possible to dynamically control the position of the driven current during the discharge as required for ITB control.
2. It was forwarded that an antenna spectrum, symmetric but less favourable concerning impurity production than that for current drive, still does not lead to impurity problems. The symmetric antenna spectrum typically used for heating in ASDEX Upgrade is produced by currents in the two antenna straps, which are 180 degrees out of phase. It is known [18, 19] that this spectrum is least likely to produce impurities. An (asymmetric) current drive spectrum will be generated by currents which are 90 degrees out of phase. Impurity production could be larger under these conditions. To test the issue, we performed heating experiments under the (for impurity production) even more stringent conditions of currents in different shapes completely in phase. Despite this, the impurity concentration was only slightly increased. This indicates that impurity production should not be a problem with a current drive spectrum.

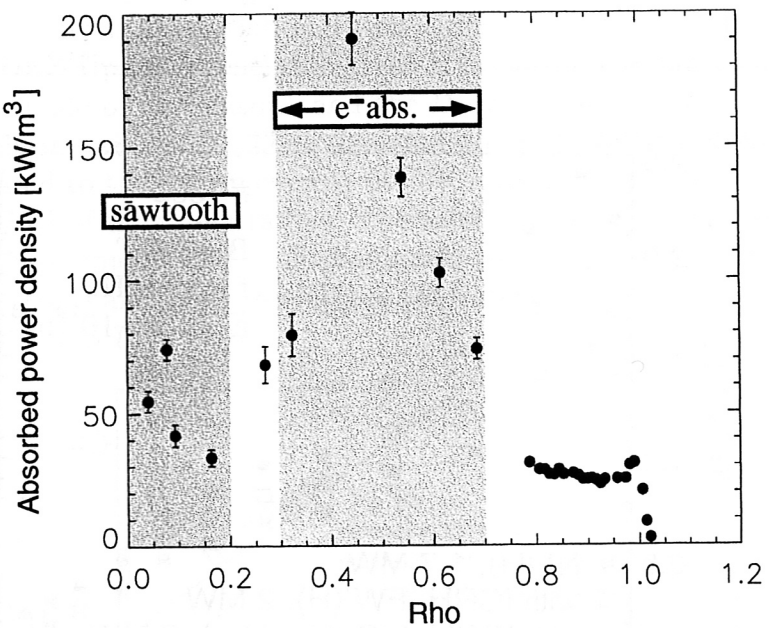

Figure 10: Power deposition profile versus in the combination ^{3}He in H.

4.1.4 Conclusions

Several options are possible to influence the current profile, as required for ITB experiments, using current drive in the ion cyclotron frequency range. Estimates indicate a driven current in the 150 kA range for 4 MW coupled to the plasma with an asymmetric antenna spectrum. Technical modification are needed to permit this type of spectrum. Pilot experiments have shown that it is possible to couple to the electrons, using scenarios envisaged for CD on ASDEX Upgrade, and that no impurity problems are expected with the asymmetric antenna spectrum.

4.2 Technical Modifications Required for Current Drive

4.2.1 The ICRF system at ASDEX Upgrade

ICRH at ASDEX Upgrade is provided by four generators with an output power of 2 MW each, transferring their power to four double strap antennas via coaxial feeding lines. This coaxial line system includes stub tuners, matching the complex antenna impedance to that of the generator output, and 3 dB hybrids, combining the generators and antennas to two double systems with two generators and two antennas each (fig. 11). The hybrids serve primarily to achieve stable and reliable operation at high power: Plasma variations, mainly at the boundary, result in a varying antenna coupling impedance, in mismatching, and in power reflections back to the generator, which reacts at least with power reduction or even with cut-off or self-oscillation. With asymmetric phasing between the straps as required for current drive these reactions are even larger. If two antennas are fed via a hybrid splitter as shown in fig. 11, symmetric reflections from the antennas are compensated, and even asymmetric ones are only partly transferred to the hybrid entrance, the other part being fed into a dummy load. The generators are thus largely decoupled from the load and the power capability and reliability of the system are greatly improved.

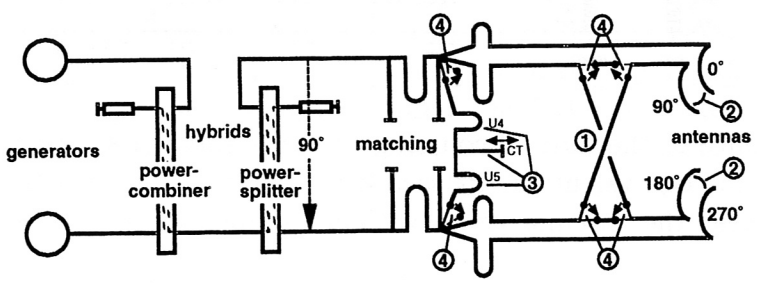

Figure 11: ICRH and ICCD circuitry at ASDEX Upgrade. For current drive the following parts must be added to the existing circuitry: 1) cross-over feeding of antenna straps, transferring the 90° phasing of the 3 dB hybrid to the antenna straps, 2) mutual coupling between antenna straps, compensated by the compensation circuit (3), which consists of two line stretchers U4 and U5, adjusting the electrical length between the branching and the compensation stub to l/4 + nl/2, and the compensating stub CT. Coaxial switches (4) allow one to choose between heating and current drive operation.

4.2.2 The current drive circuitry

If the splitter hybrid is terminated with its characteristic impedance at all its inputs and outputs as in the case of matched loads, it provides a phase difference of 90° between its outputs. This phasing is to be utilized for current drive at ASDEX Upgrade by feeding the two straps of two antennas via cross-over connections, as shown in fig. 11. But in the case of such asymmetric feeding, the mutual coupling between adjacent antenna straps must also taken into account. Its influence, which can greatly modify the launching characterisics, has been analyzed by modelling the whole RF circuitry including feeding lines, matching elements,and hybrids, the antenna being represented by simplified equivalent circuits as shown in fig. 12. Measurements of the antenna characteristics within the ASDEX Upgrade torus showed that at 30 MHz, which is the frequency chosen for current

drive, this circuit describes the characteristics with sufficient accuracy. The influence of the plasma on the mutual coupling was found to be small by applying steel wool in front of the antenna. The calculations show that the mutual coupling results in unacceptable phase variations and highly asymmetric power radiation (fig. 12). The calculations also showed that the mutual coupling can be passively compensated by the circuitry shown in fig. 12, superimposing reactive currents upon the antenna. They can be adjusted by a stub tuner, acting either capacitively or inductively, depending on the deviation from its neutral length of l/2. Since the measurements showed that the plasma influence is small, the mutual coupling is nearly given by the antenna geometry only, and the tuner must only be adjusted once before operation starts. The compensation circuit results in a small bandwidth for current drive and in higher voltages in antenna and feeding lines as compared with the symmetric heating operation. For the equivalent circuit shown in fig. 12 an increased voltage of about 15% has been calculated.

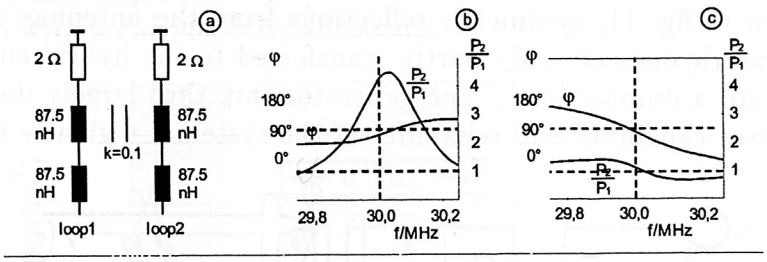

Figure 12: Influence of the mutual coupling between antenna straps with 90° phase difference: (a) antenna equivalent circuit used for the calculations, (b) the phase and power distribution between the antenna straps without compensation, (c) with compensation.

5 SUB-PROJECT 2: ADAPTION OF THE ASDEX UPGRADE DIVERTOR FOR PLASMA SHAPES WITH VARYING TRIANGULARITY AND EXHAUST OPTIMIZATION

Scientists responsible: B. Streibl, J. Neuhauser (IPP Garching)

5.1 Aims of the Divertor Research Programme

There are two major research aims for an optimized poloidal divertor in a tokamak fusion reactor or a reactor-grade tokamak experiment like ITER:

- stationary power exhaust with respect to a maximum technically feasible power load $\leq 10\,\mathrm{MW/m^2}$ on dedicated high-heat-flux components (the remote divertor target plates) and much less elsewhere

- efficient control of the plasma particle inventory and composition, in particular continuous He-ash removal at a sufficiently high rate to avoid hydrogen isotope fuel dilution.

In addition, the divertor as an integral part of the whole system contributes in more subtle ways to the overall machine performance, e.g. by controlling impurities produced at material walls or added deliberately to radiate part of the fusion power, or by allowing access to specific improved core energy confinement regimes. This inherent divertor potential is being explored in a world wide effort, in bi- and multi-lateral co-operation, and, in particular, within the ITER R&D programme as an international umbrella and coordination instrument. ASDEX Upgrade, run by IPP Garching, plays a key role in this programme.

Strict similarity (in terms of relvant dimensionless variables) between running experiments and ITER-type next-step facilities is impossible for the hot plasma core plasma [20], and even more so for the edge and divertor region, where various atomic physics processes make the physics rather complicated [21]. Any prediction for future experiments therefore requires detailed investigations over a sufficiently large parameter range, and experimentally validated models and codes for extrapolation. The former calls for a high degree of flexibility of the divertor with respect to plasma parameters and equilibrium configurations of interest in clear competition with the equally desired optimization for a specific plasma shape and operation regime. The latter indicates the need for a vigorous theoretical-numerical programme in close contact with experiment. Both aspects are discussed below in detail with reference to ASDEX Upgrade.

5.2 Recent ASDEX Upgrade Divertor Results

The experience from an extended operation period on ASDEX Upgrade with a rather open divertor (DIV I) together with numerical code simulations served as a basis to instal a deeper and much more closed divertor (called DIV II, or LYRA, because of its lyre-shaped poloidal cross-section), which has been in operation since spring 1997. This LYRA design has been optimized for specific ITER-EDA-type configurations [22] in order to demonstrate the validity of the basic divertor physics model incorporated in the B2-EIRENE two-dimensional tokamak edge code. The latter was developed jointly by IPP Garching, FZ Jülich, and New York University/Courant Institute. (This code package has meanwhile been exported to a number of other institutions in Europe, US, and Japan, and it is also used by the ITER Joint Central Team).

Figure 13 shows the LYRA divertor in comparison with the "open" DIV I. Key elements of the LYRA design are vertical target plates with rather glancing incidence of the separatrix on both targets, a roof baffle in the "private flux" region below the separatrix X-point, and strong baffling towards the main plasma chamber, accomplished by extending both target plates vertically upwards roughly along magnetic flux surfaces.

The glancing incidence of the power flowing in a narrow layer along the separatrix distributes the energy over a wider target surface area. This effect is beneficial in any case and is particularily helpful for divertor regimes where upstream volume losses are small. It is, however, precisely the volume power loss which the LYRA design intends to maximize:

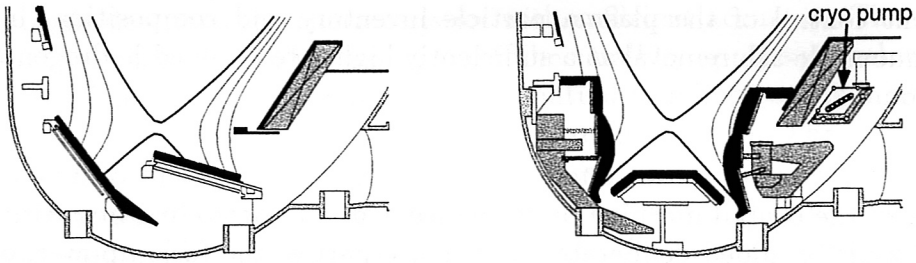

Figure 13: Poloidal cross-section of the original ASDEX Upgrade divertor (left) and of the new Divertor II (LYRA), right). The flux surfaces in these figures have a radial separatrix of 12 mm in the plasma midplane.

The inclined targets reflect the recycling hydrogen neutrals (impinging ions neutralized upon wall contact) towards the power-conducting layer, and the baffling towards the main chamber allows multiple neutral wall reflection and hence high divertor neutral pressure without direct, deleterious effect on the core plasma. The roof baffle, leaving small gaps to the target plates, was designed to maximize hydrogen and helium pumping, but also helps to concentrate the recycling towards the power-conducting layer (it also houses a selection of diagnostics necessary to analyze these complicated divertor mechanisms). In parallel to the divertor reconstruction, an internal cryopump ($100\,m^3/s$ for D_2) adjacent to the divertor (fig.13) has been installed in addition to the external turbomolecular pumps ($12\,m^3/s$ for D_2 and He). Similar arguments as for the hydrogen flow pattern hold for impurities, especially carbon sputtered physically and chemically from graphite wall components. Volume losses from hydrogen neutral-plasma interaction and, somewhat further upstream, from impurity radiation should strongly reduce the power flow arriving locally near the separatrix strike point at the target, or even extinguish it for extreme recycling accompanied by onset of hydrogen volume recombination (divertor plasma "detached" from taget plates). Instead, the power radiated before reaching the target is distributed over the whole divertor surface, resulting in much lower local power load per unit area. This overall picture has been confirmed by extensive experiments and interpretative code simulations with B2-EIRENE during the past two years. Results were presented at various conferences [23, 24] by the fusion community. Divertor modifications are being tried within the ITER R&D programme on other machines, too [25], and, as far as results are available, they seem to be consistent with ours.

5.3 Divertor Modification for Higher Triangularity and Projected Performance

There is increasing experimental and theoretical evidence that plasma shaping, especially a sufficiently strong triangular deformation (e.g. $\delta > 0.35$) of the poloidal cross-section, can significantly improve the overall plasma performance (see sec. 2). There are also indications that the favourable confinement properties at medium density can be retained with high triangularity nearly up to the empirical upper density limit (Greenwald limit [26]) or, equivalently, that the upper density limit can be raised beyond the empirical limit, which was derived mostly from low-triangularity limiter plasmas. There is also a well-documented influence oftriangularity on the size and frequency of edge-localized modes

(ELMs) in an undesired direction towards rare large-amplitude pulses with increasing triangularity. Above a certain δ value, however, the characteristic seems to change to another, small and frequent ELM type which is harmless for the divertor, or to the appearance of an "enhanced D_α regime" [27], which might be even more favourable for divertor performance.

All these effects call for a thorough study of the physics behind them by varying the plasma triangularity up to the highest possible value. Figure 4 shows a selection of possible plasma shapes with different ellipticity and triangularity in ASDEX Upgrade. While a non-baffled, open divertor like the one on top of the vessel can cope with this variation to some extent, a design which is highly optimized to a specific low triangularity single-null equilibrium like the present LYRA necessarily causes some mismatch at high triangularity, where the outer divertor leg lands on the roof baffle instead of hitting the outer target.

Preliminary experimental tests of this less favourable situation were constructed in summer 1998 by poloidally tilting a low-triangularity plasma, resulting in a significantly increased maximum power load near the shifted strike point (glowing tile edges!) in agreement with B2-EIRENE modelling. During the last maintenence period (autumn 1998) the poloidal field shaping capability was improved and the roof baffle was hardened (CFC tiles with "hidden" tile edges). High-delta equilibria can now be routinely run, but again with the outer leg on the LYRA roof baffle. According to the above-mentioned pre-experiment, we may expect increased heat load problems and worse divertor performance, eventually masking beneficial core plasma effects from increased shaping parameters.

Though some mismach between divertor and plasma shape with varying triangularity cannot be totally avoided, we can try to minimize the effect over a reasonably wide range by re-designing the divertor while retaining the key features of the LYRA divertor outlined earlier: The inner target is kept with minor modification of the upper part, while the outer target and the roof baffle are reconstructed such as to fit best to some high triangularity value. In principle, we retain the qualitative divertor characteristics, but relax some of the LYRA optimization criteria (less glancing target incidence, less accurate fitting into the pumping slits, ...), still requiring that both pumping slits always remain in the private flux region for all configurations of interest. In this way, we may reduce the degree of optimization, but gain by reducing the sensitivity of the divertor performance to plasma shape variations.

In order to check the validity of these assumptions and in preparation for a final design, a set of typical equilibria with different triangularity, combined with either the present LYRA and a modified divertor (not yet the final design, but close to it), were investigated with B2-EIRENE using physics model parameters derived from previous experiment analysis [28]. Figure 14 shows a selection of cases: the LYRA divertor with a low-triagularity plasma (fig. 14a), the new divertor with the same low-triangularity equilibrium (fig. 14b), and the new divertor with a high-triangularity plasma (fig. 14c). There are necessarily many local differences in the divertor behaviour between these cases, which cannot be discussed here in detail. However, a few rather clear conclusions can be drawn from this preparatory study: The low-delta equilibrium fitting optimally into the LYRA (fig. 14a) also behaves rather well if combined with the modified divertor. In fact, for a plasma with a power of 12 MW into the edge, a separatrix density of $3 \cdot 10^{20}\,\mathrm{m}^{-3}$ and

2.5% chemical carbon sputtering, the maximum power load is around 1.5 MWm^{-3} in both cases, with the overwhelming part of the input power radiated before reaching the target. A high-triangularity plasma fits the new divertor rather well anyway (fig. 14c) and has characteristics close to the case in fig. 14a, as expected.

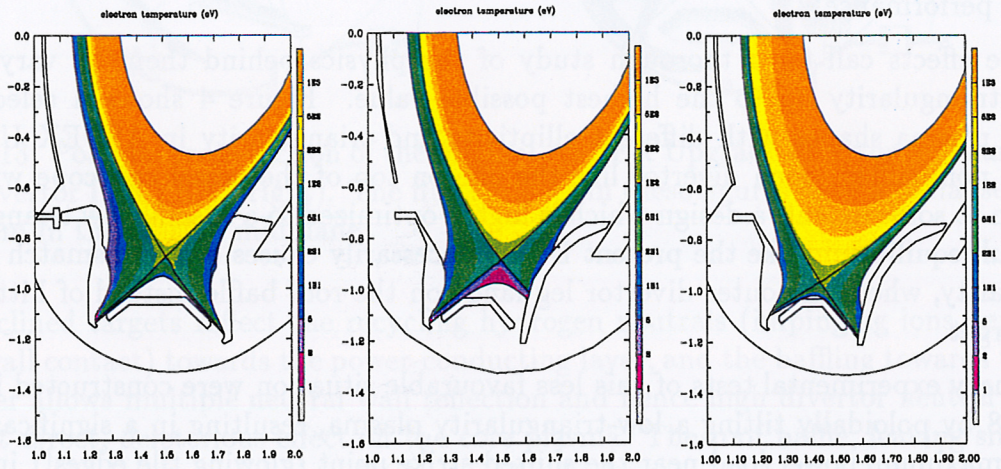

Figure 14: Examples of electron temperature contour plots for different divertor and plasma configurations as calculated with the B2-EIRENE code package. Analysis of the present LYRA divertor with a low-triangularity plasma (left) was used to check and validate the physics model. The code was then used to assess the performance of modified divertor structures with low (middle) and high (right) triangularity. The divertor shape shown here is already close to the one finally chosen.

5.4 Proposed Changes on the Plasma-facing Divertor Components

The main goal for DIV II (fig.15) was to achieve a low heat flux density on the target plates near the strike point of the separatrix by means of impurity radiation and a small acute angle (12.5°) between the separatrix and target. To reach this goal safely the longest possible divertor fans were aimed at. As a consequence, the divertor had to be designed for a specific bottom triangularity ($\delta_{bot} \approx 0.3$) and could not cope with relevant triangularity variations. Our results (see sec. 5.2) have in the meantime shown that compromises are possible with respect to the acute angle and fan length. As long as a major part of the recycling gas efflux is directed towards the hot separatrix zone, there is always a remarkable reduction (factor $\approx$ 2) of the heat flux density compared with horizontal plates.

It is thus possible to rebuild the LYRA (DIV II) for a large bottom triangularity ($\delta_{bot} \leq 0.5$) in combination with a reasonable triangularity variation ($\delta_{bot} \geq 0.3$). The rebuild of the LYRA required to achieve these goals will be referred to as Divertor IIb (DIV IIb). DIV IIb is shown in fig. 16 together with the already existing LYRA. The required changes of the LYRA target result from the inward shift of the stagnation point (X-point) in combination with an inward rotation of the whole separatrix around the X-point. The two effects are coupled and rise with the bottom triangularity. For mainly vertical inner and outer targets a triangularity variation is thus always accompanied by a vertical movement

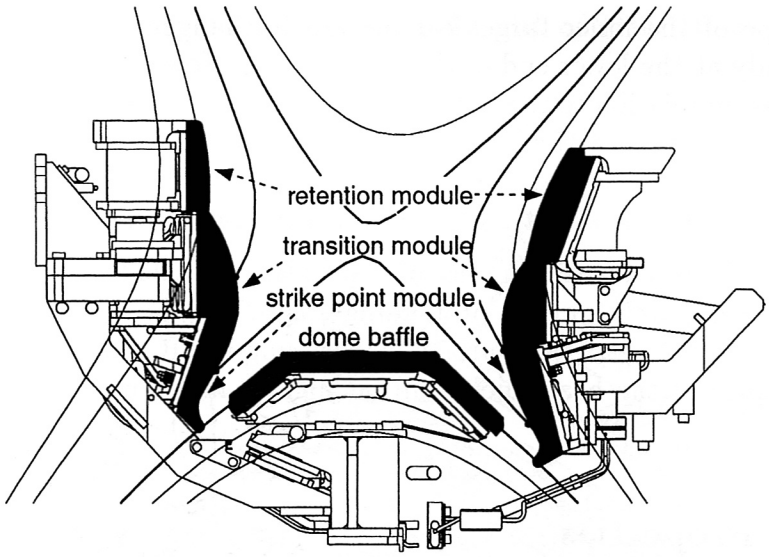

Figure 15: The existing Divertor II, called LYRA

of the strike points. This movement is opposite for the outer and inner strike points and less pronounced on the inner target. The range of the movement can be judged from fig. 16, where the divertor fans are shown for both extreme conditions, i.e. for $\delta_{bot} = 0.3$ corresponding to the LYRA, and $\delta_{bot} = 0.5$, driving the rebuild.

To keep, for high δ, the heat flux of the outer separatrix fan away from the roof baffle, the outer target together with the adjacent wall of the roof baffle has to be shifted much further inside. To allow a triangularity variation towards lower values, the outer strike point for $\delta_{bot} = 0.5$ has to be located at the bottom end of the new outer target plate. To facilitate feedback control of the strike point location, a plain shape is now chosen for the target plate over the whole region of the envisaged strike point positions.

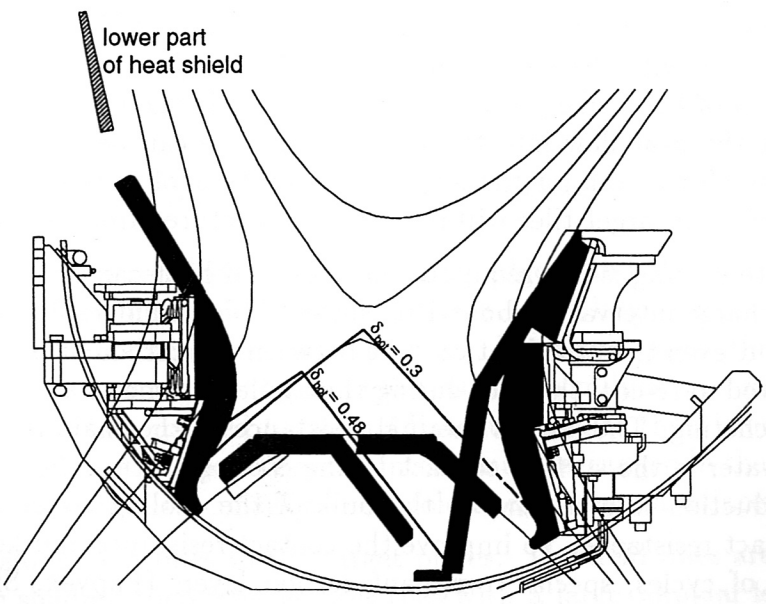

Figure 16: Transition to the new divertor IIb. Black contours show DIV II, shaded contours DIV IIb.

The general shape of the inner target can be left unchanged since the strike point for $\delta_{bot} = 0.3$ is already at the lower end of the target plate. Towards larger triangularity the strike point moves, in relation to the outer target, only slightly upwards. The major effect is an appreciable reduction of the inner divertor fan length. However, this is acceptable since the heat flux to the inner target is less than 40% of the total heat flux to the target (the total target heat flux is about 25% of the heating power).

The shape of the LYRA transition modules (baffles) will be considerably changed to avoid intense recycling on the upper protruding edges. On the outer target there will be a smooth transition to the last flux surface just passing the ICRH antenna. For the inner target the lower part of the heat shield will be slightly more inclined to avoid a leading edge on the baffle.

5.5 Design Properties

The LYRA has hitherto been successfully operated over a period of one year. Even at the maximum additional heating power of 20 MW no problems were encountered in the region of highest heat flux with hot spots and the resulting carbon sublimation. The LYRA has also survived a great number of hard disruptions. All components of DIV IIb to be rebuilt will therefore be realized with technical solutions already developed for the LYRA divertor. Development cost will thus be saved and the cost and time estimates can be based on the experience with the LYRA construction. The technical solutions of the LYRA have been approved for EURATOM preferential support phases 1 and 2 in 1994 and are described in detail in [29]. In the following, a short description of major design features will be given.

5.5.1 Heat removal and edge shading

Experimental evidence shows that the heat flux density on the critical outer target stays below 4 MW/m^2 even with the upper limit of the additional heating power being 20 MW. Vertical movement of the strike point by 10 cm did not change this favourable result [24]. This means that the heat flow into the most critical tile can be absorbed adiabatically with fine-grain graphite, even for the longest flat-top time of $\approx$ 10 s (which is limited by the power supply). All target tiles will thus be manufactured from fine grain graphite.

Since steady-state cooling is not required, the absorbed heat can be removed during the much longer discharge interval of about 10 minutes. This considerablyreduces the cooling requirements. But even then the heat contact between the carbon tiles and cooling plates has to be improved to re-cool the tiles during the available time to about 100^0 C, allowing temperature ratcheting. The largest thermal resistance on the chain from the carbon tile to the cooling water is the surface contact to the cooling plate. The thermal resistance of the heat conduction in steel and to the bulk of the cooling water can be neglected against the contact resistance. To improve the contact resistance and keep it stable over a large number of cycles, special compliant carbon layers (Papyex, Sigraflex ....) are inserted between the tiles and the cooling plates to increase the heat transfer area. For the strike point tiles these layers are tapered by machining to achieve the inclination for edge shading. Edge shading will also be applied beyond the strike point region, but only

in front of the large diagnostic slits with a toroidal width of 20 mm to avoid leading edges there.

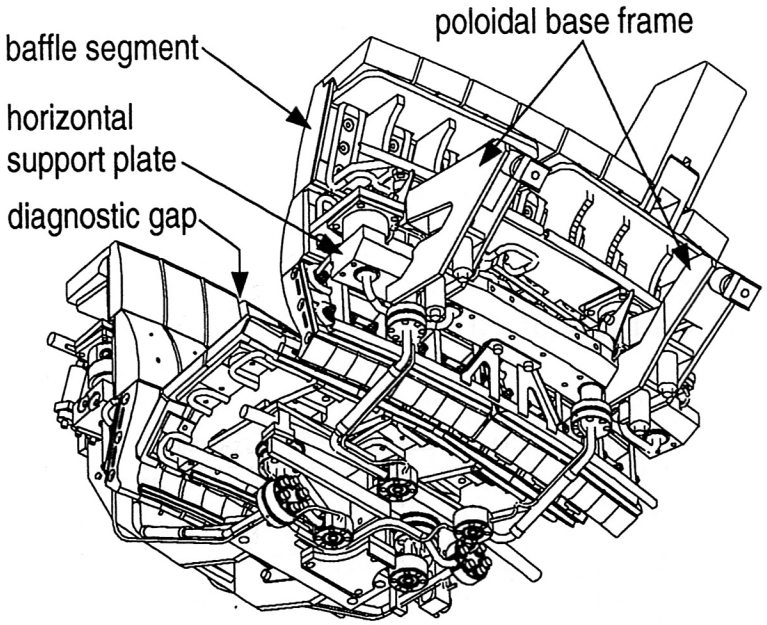

Figure 17: Module structure of the LYRA divertor. The cooling circuity is also shown.

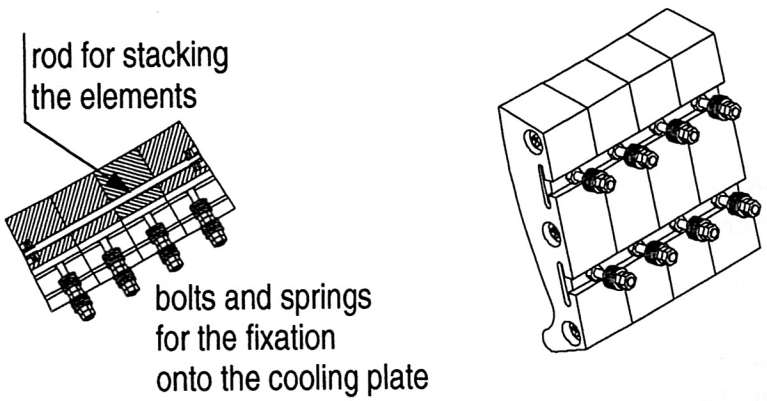

Figure 18: Stacked design for strike point tiles.

Edges shading is mainly required to avoid leading edges (and the resulting carbon sublimation) resulting from dimensional misalignments. The largest misalignments are encountered between the detachable target modules. For them dislocations normal to the tile surface cannot be kept smaller than a few tenths of a millimetre (± 0.15 mm). Larger tile gaps also have to be accepted between adjacent modules than inside a module. An exception are the diagnostic gaps. They are intentionally arranged in the middle of special modules (fig. 17) to reduce the misalignment tolerances between adjacent tiles.

The heat flows along field lines to the target plates. The field lines are directed mainly toroidally. Edge shading therefore requires tiles with a large toroidal length. Otherwise the ratio of shaded to heated area becomes too large. For the LYRA and DIV IIb the outer target tile length chosen is about 160 mm. For these tiles the increase of the heating flux density due to the tile inclination can be kept below 20% with the achievable tolerances

and required structural gaps. But long tiles warp considerably under high heat loads. The tiles of the strike point region are therefore subdivided in the toroidal direction into four small units about 40 mm long, stacked together by rods (fig. 18). Each unit of a tile is clamped to the cooling plate. In this way the warping becomes negligible though the tile integrity is maintained. The inclination required for tile shading is mainly defined by the tolerances normal to the cooling plate, but also the gap width between the tiles contributes markedly. The gap sizes have therefore been reduced in relation to the LYRA. Between adjacent tiles of the same cooling plate they are now only 2 mm, and between modules 4 mm.

5.5.2 Base frame and module structure

All divertor components have to withstand strong magnetic forces caused by major plasma disruptions. Sizeable support structures are therefore required. The LYRA stainless-steel support structure consists of two parts, the lower base frame (fig. 15) and the target supports (fig. 17). The base frame is the link between the target structures of a module and the wall of the plasma vessel. All module structures are fixed solely onto the base frame. The base frame is thus the dimensional reference and will not be altered for DIV IIb, thus keeping the geometrical reference.

An assembled module of the LYRA divertor is shown in fig. 17. The same concept will be applied for DIV IIb. According to the basic design of the vacuum vessel there are 16 sectors arranged around the toroidal circumference. To approximate the toroidal curvature more precisely for reduced machining effort on the carbon tiles, the toroidal polygonality is raised to 64 by introducing an additional 4 polygon traces within each target module. Stiff segment plates reinforced by bulkheads carry the carbon tiles. Each segment plate is directly cooled via a cooling pipe meander. The circular shape cooling pipe is brazed into a machined groove to provide good thermal contact to the plate.

The water manifolds are integrated in horizontal extensions connected with the tile holder plates to combine quick mounting with intense cooling. The lower two modules are bolted to the horizontal support plate, which forms the toroidal connection of the two poloidal base frames. The water manifold connections are tightened via tow edge rings, which are arranged in the centre. The inner edge ring seals the water. The outer edge ring provides an intermediate vacuum. To support the upper baffle module, beams with rectangular cross-section are welded to the horizontal support plate. The baffle module cooling plate is fixed at the upper end of these beams. The vertical beams are joined by stiffeners to the poloidal base frame in order to take up effectively the moment created by halo currents. The cooling water of each of the 10 modules enters via the feed-through at the bottom of the vessel. Each module is fed in parallel and the total flow of the inner and outer target cooling circuits enters through the corresponding horizontal support plates. The cooling circuits of the inner target and the roof baffle of a module are switched in series. The outer target of each module has an independent cooling circuit.

6 SUB-PROJECT 3: EXTENSION TO HIGH-FREQUENCY OPERATION OF THE DYNAMIC ERGODIC DIVERTOR (DED)

Scientists responsible: K.H. Finken (FZ Jülich)
The dynamic ergodic divertor (DED) for TEXTOR-94 is expected to provide new and unique features of tokamak operation. Its integration into TEXTOR-94 is planned in two steps: (i) a DC and low-frequency system already under construction and to be implemented in the year 2000; (ii) an extension to high-frequency operation (1 kHz to 10 kHz), which is the subject of the present application.

After a technical description of the dynamic ergodic divertor as a whole, some basic features of the plasma edge as influenced by the DED are addressed, namely the enhanced transport in the ergodic layer and the widened heat flux pattern hitting the wall through the laminar zone. On the basis of this general introduction into the principle of the DED, some specific aspects of the scientific potential – being the subject of this application – of the high-frequency operation are discussed. These are (i) magnetic field line reconnection in an ergodic layer, (ii) torque transfer from the external perturbation currents to the plasma, (iii) formation of an internal barrier in order to improve the energy confinement, (iv) unlocking of modes in order to expand the operational limit of a tokamak, (v) stabilization of internal modes by a feedback system, and finally (vi) optimization of particle removal by the rotating field.

6.1 Descriptions of the DED Base Version and its High-frequency Extension

The main component of the DED is a set of magnetic perturbation coils to ergodize the magnetic field structure in the plasma edge region; these coils are located inside the vacuum vessel at the high-field side of the torus, as shown in 19. Fourteen contributions to the design and physics questions are given in [30]. The set consists of 16 individual coils (4 quadrupoles) plus two compensation coils. The individual perturbation coils, each with one winding around the torus follow the direction of the equilibrium magnetic field of the plasma edge (i.e. helically); this procedure produces a resonant enhancement of the effect of the external perturbation field on the edge plasma. A perturbation current of only 15 kA is therefore sufficient to create a stochastic boundary (the 15 kA has to be compared with a plasma current of Ip = 500 kA or with the current that would be required to energize a poloidal divertor, which is of the order of Ip).

The free ends of the individual coils are fed to the outside of the torus, freedom being provided to connect them to the individual power supplies in various manners. In order to avoid (i) vertical instabilities and (ii) modification of the pre-programmed plasma current, the net current flowing in the perturbation coils should be zero. In its basic operational mode, neighbouring coils of the DED have a current phase shift of 90°.

In the plasma edge the resulting perturbation field excites modes with fourfold toroidal

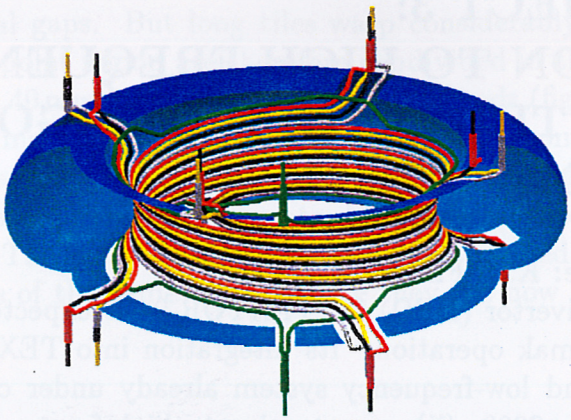

Figure 19: Scheme of the DED coils.

symmetry (n = 4) and with about 5 major poloidal mode numbers centred around the major mode m = 12. The dominant mode becomes resonant at that radial layer where the safety factor is q = m/n = 3, i.e. close to the edge as desired. This main mode (m/n = 12/4) was selected because it creates only small local perturbations (magnetic islands) and does not lead to undesired disturbances in the plasma core. By connecting some perturbation coils in series, also coarser modes (m/n = 6/2 or 3/1) can be excited. They provide a higher degree of ergodization in the plasma edge but they also penetrate deeper into the plasma core (desired only for few specific purposes). The basic mode of operation will therefore be the 12/4 mode. However, the power supplies and the specific connection system also allow one to superimpose on the 12/4 mode a minor fraction of the 6/2 mode, thus providing an attractive combination of ample edge ergodization together with yet unperturbed core plasma.

The envisaged phase shift of 90° between the currents in neighbouring coils is achieved by a 4-phase power supply system. Such a 4-phase system has the advantage of easily also permitting DC-operation and, since the next but one coil carries the return current of the first one, it does not require an additional power supply unit. When operated by an AC current, the perturbation coils create a propagating magnetic field similar to that of an AC motor. This propagating field is predicted to produce two new beneficial effects: (i) The local heat flux pattern created on the plasma-facing components – showing a strong spatial modulation in the case of DC operation of the DED – will be swept over the whole surface, thus leading to the desirable equidistribution and (ii) it will transfer a torque to the plasma edge just as expected from the simple motor picture. While a low-frequency rotation of the perturbation field is sufficient (f = 1 kHz) to equidistribute the heat flux, the applied torque will become relevant at higher frequencies only: sheared plasma rotation is one tool to reduce turbulence.

The whole DED system, i.e. including high-frequency operation, was planned such that the in-vessel coils and the main power supplies (belonging to the basic equipment) are already designed to cover the full operational range. The present application therefore concerns only those components of the DED system which are specifically required to extend the frequency range from 1 kHz towards 10 kHz. These are the capacitor banks compensating the inductive load of the DED coils at 7 selected frequencies within this

range, transformers, switches, cables, and the respective commissioning. Technical data are given in table 1.

Frequency	Max. current
1 kHz	15 kA
2 kHz	10.6 kA
3.1 kHz	10.6 kA
4 kHz	10.6 kA
5 kHz	7.5 kA
7.5 kHz	7.5 kA
10 kHz	7.5 kA

Table 1: Maximum currents at envisaged frequencies. Additionally, the perturbation current can be applied in the whole frequency band up to 10 kHz at a reduced amplitude of 1.5 kA.

6.2 Features of the Static and Quasistatic Operation

Before addressing the high-frequency aspect of the DED, some properties of the static or quasi-static operation (upon which the high-frequency extension is built) are described. Being exposed to the applied perturbation field, the following three zones of the plasma can be distinguished: The inner section of the plasma column (about 90% of the radius) will be influenced by the perturbation field only weakly or not at all and consequently will retain its good confinement properties. This inner section will be surrounded by an ergodic layer which has a thickness of a few centimetres only. The outermost layer, finally, is called the laminar zone; it is characterized by open magnetic field lines intersecting the divertor target plate.

6.2.1 The ergodic layer

The ergodic layer is created by those spatial Fourier modes (characterized by the poloidal and toroidal mode numbers m and n) of the perturbation field which are resonant to a magnetic surface (characterized by the safety factor q and the radius r) of the considered area such that q=m/n. The m/n mode of the perturbation field creates a magnetic island around the resonance radius with an island width proportional to the square root of the perturbation field amplitude. If the perturbation field contains several spatial Fourier modes, each of them will establish an island on "its" resonant magnetic surface. As long as the island widths are small as compared with the distances of the islands, the islands are isolated and do not (in first-order approximation) influence each other. The magnetic surfaces are deformed in a characteristic way by the islands but they still remain intact KAM (Kolmogorov, Arnold, Mozer [31]) surfaces. An example of this situation is shown in fig. 20a for a low perturbation amplitude of the DED field. For obtaining a higher radial resolution, the axes are the poloidal angle and the minor radius from 40 cm to 50 cm

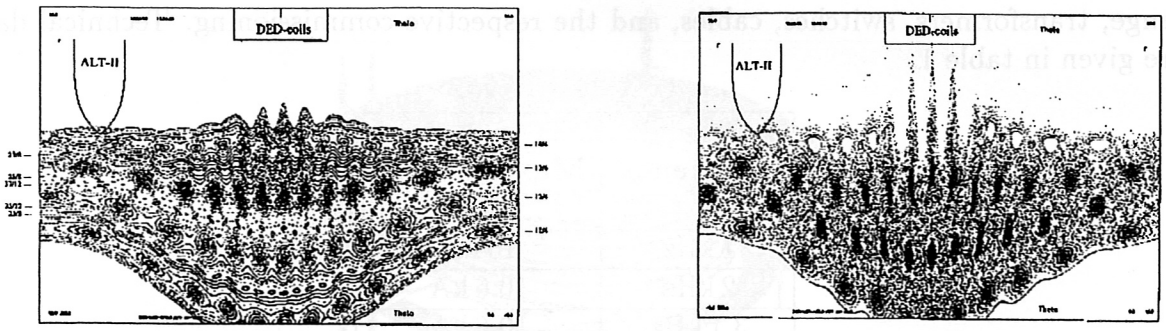

Figure 20: Poincaré plots for wealy (a) and fully (b) ergodized plasma edge. The horizontal axis is the poloidal angle from 0 ... 2; the vertical one is the minor radius between 40 cm and 50 cm. Poincaré plots are constructed by field line tracing; each intersection of a field line in a poloidal cut is marked by a dot.

(the normal minor radius of TEXTOR-94 is 46 cm). We observe four dominant magnetic modes, namely n = 4 and m = 11 ... 14 (right label). In addition, also higher modes can be found as marked by the labels at the left side. The picture is a so-called Poincaré plot, an important illustration technique in non-linear dynamics. It is obtained from magnetic field line tracing where the intersection points of the field line with a chosen poloidal cut are marked. If the perturbation field becomes so large that the islands start to overlap, the system becomes ergodic. This means that the magnetic field lines are no longer restricted to surfaces but fill a volume. Field lines "diffuse" through the whole ergodized area. The field line diffusion is linked with enhanced radial plasma transport is this area; the transport enhancement was the starting point to propose ergodization as a means to mitigate the otherwise extremely high power flux density to plasma-facing materials in a fusion reactor. A picture of the fully developed ergodic structure in the boundary of TEXTOR-94 is shown in fig. 20b. The ergodic layer has been intensively modelled both qualitatively by the Poincaré plot technique and quantitatively by statistical methods for the whole operational space of the DED [32, 33].

6.2.2 The laminar zone

The laminar zone is a specific feature of an open ergodic system. An intuitive example is the billiard game on a racetrack type of field: the successive orbits of the ball are chaotically distributed; if part of the reflecting wall is removed (open system), some orbits are no longer populated or lead to quick loss of the ball. In a similar manner, the ergodic structure of the plasma edge imposed by the perturbation field is also open: Particles attached to those field lines which intersect the divertor target plate are neutralized there. The field line tracing process is therefore stopped at this location: The "open" field lines as defined by this procedure form the laminar zone. In contrast to the ergodic zone, the field lines of the laminar zone are well ordered. Characteristic areas can be found where all field lines have similar properties, e.g. a similar connection length between two intersections at the divertor target plate. We visualize this property in the poloidal plane as shown in fig. 21, using a similar presentation as was used for the previous Poincarè plots. Because of the multiple symmetry of the DED, only one of the periodic sections of the poloidal angle need be shown. Different colours represent different connection lengths

of the field lines. The large blue area stands for field lines with a connection length of about one poloidal turn (i.e. $L = 2\pi R_0$) and the green area represents those field lines which go poloidally twice around the torus before intersecting the target plate. Lines with an even longer connection length form smaller areas and gradually merge with the ergodic sea (black).

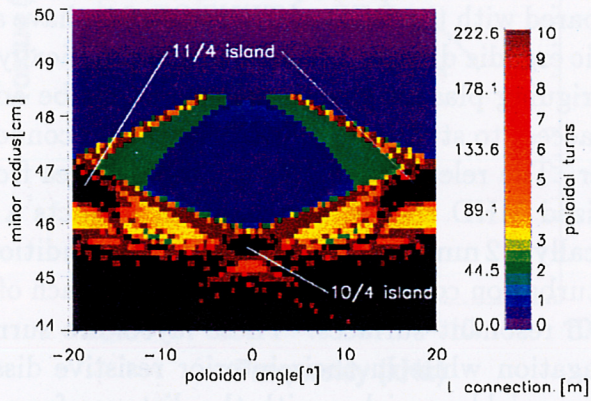

Figure 21: Connection length of the magnetic field lines marked at the low-field side

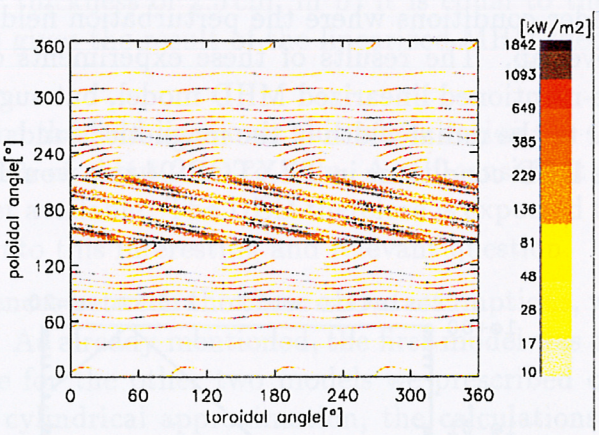

Figure 22: Heat deposition pattern on the wall; the helical strike lines are just in front of the DED coils

In general, modelling the plasma transport inside the ergodized edge is extremely complicated. The relatively large areas of similar structure in the laminar zone, however, allow to derive a simplified plasma transport model to be derived by applying conventional scrape-off layer treatments for each of the different areas. In this way, we have treated the laminar zone by means of 1D and 2D models and are now even testing a 3D model. One result of such modelling is the heat deposition pattern on the divertor target region caused by the power flow to the wall as shown in fig. 22. The plasma of areas with double poloidal connection length introduces a convective exchange path for heat and particles. In keeping with the geometrical arrangement of the DED magnetic coils, the heat is deposited along 8 helical strike lines. Enforcing a low-frequency rotation of the DED field, the heat load will be equidistributed over a large area, thus reducing the local (averaged) heat load density to a tolerable level.

6.3 Features and Issues of High-frequency Operation

6.3.1 Field line penetration and reconnection

The high-frequency operation of the DED addresses further and even more exciting new physics than the static or quasistatic operation. While static ergodic divertors – though in different setups as compared with the DED of TEXTOR-94 – have already been applied to various devices, dynamic ergodic divertors have hitherto practically not been investigated. Moreover, new and intriguing plasma physics questions can be addressed. One of these concerns experimental access to study the penetration and reconnection of magnetic field lines in an ergodic layer. The relevance of this question ranges from tokamak physics to astrophysics. A linearized MHD theory, for example, predicts a sequence of very thin interaction layers (typically 0.2 mm thick for TEXTOR-94 conditions) located in the edge region between the perturbation coils and the core plasma. Each of these layers is centred at one of the typically 5 resonant surfaces. These layers are surrounded by zones with Alfvén type field propagation while in their interior resistive dissipation prevails. The effect of the Alfvén layer quickly vanishes with the distance from the resonance zone so that only the vacuum solution persists.

We know of only one experiment addressing the field line penetration. It was performed at the TEXT tokamak under conditions where the perturbation field creates islands which, however, do not yet overlap. The results of these experiments do not agree with the prediction of the above-mentioned linearized MHD model, but suggest a thickness of the dissipation layer similar to the radial width of the magnetic islands as obtained in vacuum approximation. For the DED conditions in TEXTOR-94 this would amount to a thickness of typically 5 mm.

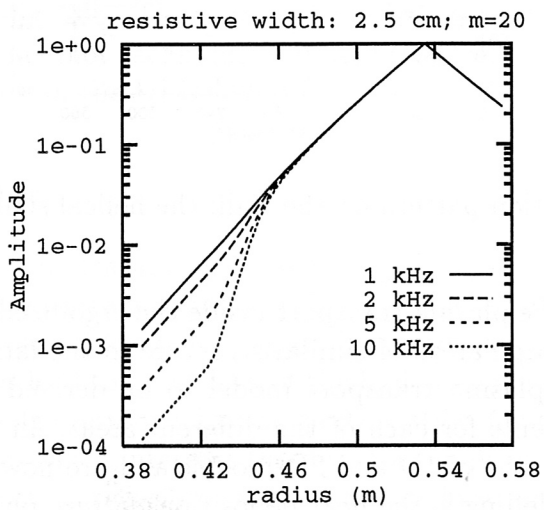

Figure 23: Radial dependence of the perturbation field amplitude; the parameters are different operating frequencies of the DED. The amplitude is normalized to 1 at the coil location.

One may argue, however, that under fully ergodized conditions the characteristic width of the dissipation layer will extend over the whole ergodic zone because the rotating field has

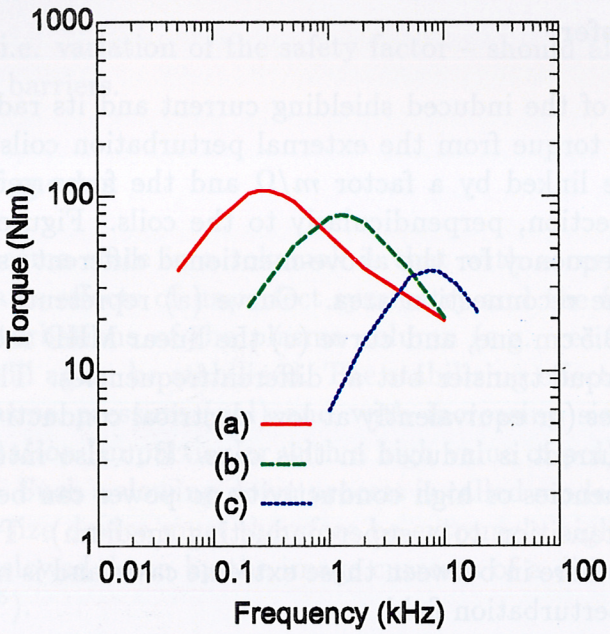

Figure 24: Torque transfer from the DED field to the plasma for three models as a function of the frequency. In model a) the dissipation layer thickness is assumed to be equal to the ergodization layer thickness of 2.5 cm, in b) it is equal to the island layer thickness (0.5 cm) and model c) gives the result of the linearized MHD theory.

to break and recombine the field lines over this whole region. In this case the dissipating area would have a width of about 2 cm to 4 cm. A self-consistent non-linear treatment of this situation is not yet available. The DED therefore is expected to provide experimental evidence and insight into this interesting and relevant question.

To quantify the differences between the three above assumptions, we modelled them as far as possible at present. As already mentioned, the first model was treated in the linearized MHD approach, while for the other two models we prescribed characteristic skin layer thicknesses. Using a cylindrical approximation, the calculations yield the radial decay (and shielding) of the applied perturbation field including the induced shielding current and the torque transferred from the external field to the edge plasma. Figure 23 shows the radial dependence of the amplitude of the perturbation field for four different frequencies assuming a thickness of the shielding layer of 2.5 cm and a plasma temperature of 50 eV (consistent with the modelling of the laminar shielding, while at 10 kHz the shielding factor exceeds one order of magnitude. (This is also of relevance to the application of the coarser but more efficient modes, which – without shielding – would negatively affect the confinement in the core plasma.) For the other two models, i.e. for a smaller skin width, the shielding factor is of course considerably smaller.

For the interaction strength (in order to induce plasma rotation) not only is the shielding amplitude important, but also the phase shift of the shielding current. This phase variation is rather sensitive and has a finite value in all cases.

6.3.2 Torque transfer

A direct consequence of the induced shielding current and its radial distribution is the transfer of power and torque from the external perturbation coils to the plasma. Both transfer quantities are linked by a factor m/Ω and the force generating the torque is oriented in helical direction, perpendicularly to the coils. Figure 24 shows the torque as a function of the frequency for the above-mentioned different assumptions concerning the current flow in the reconnection area. Curve (a) represents the 2.5 cm skin-width model, curve (b) the 0.5 cm one, and curve (c) the linear MHD model. All models show a maximum of the torque transfer but at differentfrequencies. The low torque transfer value at low frequencies (or equivalently at low electrical conductivity) is trivial because only little shielding current is induced in this case. But also intuitively obvious is the fact that at high frequencies or high conductivity no power can be transferred (take the extreme case of the transition to a superconducting medium). The maximum transfer therefore occurs somewhere in between these extreme cases and is not connected with the best shielding of the perturbation field.

In present experiments, a reference torque leading to a plasma toroidal spin-up is produced by the neutral beam injection heating (NBI) and amounts to a few Nm. The expected value of the torque applied to the plasma by the DED coils is substantially larger for all cases in the frequency range between 1 kHz and 10 kHz. However, only that fraction of the exerted force which points in toroidal direction can be compared with the NBI case; this fraction is about 10% of the total force. Even then and for all assumptions, the torque should be sufficiently large to impose a relevant differential plasma rotation and the chosen frequency may become a knob to adjust the thickness of the sheared layer.

Measurement of the frequency dependence of the transferred force should reveal the underlying mechanism of the field line and thus give an experimental clue to understanding reconnection processes in an ergodic layer. It is less clear whether the torque applied by the perturbation coils will even excite a plasma rotation in the poloidal direction because this strongly depends on the (neoclassical) poloidal damping rate and nonlinear effects.

6.4 Expected Plasma Effects

6.4.1 Internal barrier

The torque from the DED field will act on the resonant surfaces, i.e. on the plasma edge; the direction of rotation can be freely chosen. The NBI force acts predominantly in the plasma core; simultaneous application of both torques should therefore result in a rather sheared rotation flow pattern of the plasma. It is a common assumption in plasma physics that such sheared rotation is a key element for suppressing large-scale turbulence cells, which determine the anomalous radial transport. Under favourable conditions it is possible to create barriers inside the plasma which reduce the excessive transport losses. According to experimental data and theoretical interpretations, these barriers are based on radial electrical fields and sheared flows. It is therefore expected that operating the DED at high frequencies is a novel tool to reach and study advanced scenarios with internal barriers and improved confinement. An adjustment of the applied frequency and

the plasma current, – i.e. variation of the safety factor – should allow fine tuning of the radial location of such barriers.

6.4.2 Unlocking of modes

The desired normal plasma state in a tokamak is that with a certain toroidal rotation. Such a rotation mitigates effects of imperfect symmetry and the finite resistivity of the wall. In this way perturbations of the plasma column (e.g. resistive wall modes) will not further grow but will again be stabilized. The stabilizing effects become weaker with increasing internal plasma pressure (pol) and with increasing size of device. Slowing down of the plasma rotation (in particular with a high value of pol) will therefore lead to a disruptive instability. Such a slowing-down process is called mode locking. The required symmetry of a reactor-size device must therefore be extremely high in order to avoid the plasma rotation being slowed down by the image currents of a disturbance in the plasma wall ($B_{pert}/B_{tor} \leq 10^{-5}$).

Possibly, such mode locking can be avoided by imposing an external torque upon the plasma (as modelled for the high-frequency DED operation). The rotation frequency should be of the order of or higher than the diamagnetic drift velocity. The envisaged operation frequencies of the DED and the coil interconnections were selected such that they meet the relevant range required for suppressing mode locking. Since for ITER-like devices NBI will be applied at angles unfavourable to torque transfer, the proposed scheme may also be of interest and relevance for such devices.

6.4.3 Resonant interaction with internal modes

One way of suppressing resistive wall mode instabilities (RWI, ideal or resistive kink and/or tearing modes) is the enforced plasma rotation discussed in the last section. The other option discussed in the literature is resonant interaction with the modes. For this purpose, both a sensor and a feedback system are required for supplying an outer coil array with currents of the correct amplitude, frequency, and phase. The growing mode may then be suppressed and stabilized. Since the process is resonant, the required feedback amplitude is minimum.

For investigations of this kind, the DED coil arrangement and power supplies are suitable; for the low-amplitude operation the full frequency band between 1 kHz and 10 kHz can be used. Although only a few relatively coarse modes may be stabilized with this scheme, these coarse modes are the most dangerous ones so that such investigations are of great interest to the fusion community. (This point was of particular interest to the EURATOM expert group).

6.4.4 Optimization of pump limiter performance

The possibility to induce even a poloidal rotation by the torque from the DED coils is still controversially discussed; it may be facilitated by the application of a radial electric field at the plasma edge. However, if such a rotation occurs, it could be utilized to compress the particles in front of the scoop entrance of the toroidal pump limiter of TEXTOR-94

(ALT-II). The pump limiter has openings below the blades where it accepts particles from the plasma. The particle compression in front of these openings would be very favourable because it could further increase the pumping performance beyond the level achievable under non-DED conditions. This removal performance is essential in a reactor in order to remove the helium ash from the fuel. Up to now, these questions have been studied extensively within the pump limiter programme; for some regimes of operation a sufficient removal rate of helium has been demonstrated while for the otherwise best operation conditions of TEXTOR-94 further improvements in the particle exhaust are highly desired.

7 SUB-PROJECT 4: FAST SOFT X-RAY IMAGING

Scientists responsible: G. Fuchs (FZ Jülich)
A fast imaging system with a framing rate of up to 1 MHz for the spectral range of soft X-rays (0.8 to 20 keV) is proposed. This imaging system is to be used to diagnose plasmas of fusion devices. The experimental results, viz. fast picture sequences with a resolution never previously obtained from soft X-ray emission, are expected to boost the understanding of many open questions in toroidal fusion devices relating to instabilities and stationary operation. The system is now presently being designed at Institut für Plasmaphysik, Jülich, together with the partners from Princeton and Nagoya. It will first be tested on the tokamak TEXTOR-94, where first investigations of such phenomena as disruptions, sawteeth, marfes, and pellet ablation will also be conducted. Later the system is also to be used on the W7-AS stellarator.

7.1 Description of the Project and its Goals

Soft X-ray imaging is considered to be one of the crucial tools in th diagnosis of high-temperature plasmas in magnetic confinement experiments. It provides pictures of moving plasma phenomena. However, the method that has been used in fusion research up to now is still not ideal, since it affords only poor angular resolution. In present-day X-ray imaging several linear diode arrays view the plasma in a poloidal cross-section. Although several hundred diodes may be involved, the spatial resolution is still rather limited because for practical reasons there can be only a limited number (< 10) of arrays.

Phenomena with short time scales and detailed structures are of key importance for understanding instabilities in hot plasmas and for their applications nuclear fusion. In particular we think of:

- Disruptions of the plasma current: These violent plasma instabilities, which result in a complete loss of plasma confinement and termination of the plasma discharge, must be avoided in order to guarantee safe operation of a reactor.
- Sawtooth instabilities: These important instabilities affect the central plasma core of a tokamak reactor and are preceded by an $m/n = 1/1$ kink or tearing mode. They have been known for 24 years, but are notyet fully understood. In particular, no

consistent and satisfactory explanation of the fast crash – a sudden flattening of the temperature and density profiles within the plasma core – has been agreed on.
- The camera system will be used on stellerators in order to investigate stationary magnetic islands caused by field errors, for the divertor and for GAE modes.

There are a few other applications which do not necessarily employ soft X-rays but may better be done in other spectral ranges. These are: pellet injection, MARFEs, and the dynamic ergodic divertor.

The theoretical models for the various instabilities which have been put forward so far give partly contradictory results. This new experimental evidence is necessary for clarification. We propose a new camera system that will be used as a diagnostic tool (first on TEXTOR-94) to address questions where high resolution, both in space and time, is required.

7.2 Placement within Fusion Research at Jülich and Other Sites

Forschungszentrum Jülich has a research programme on thermonuclear fusion. The key instrument for this research is the TEXTOR-94 tokamak machine. Most of the above-mentioned research goals are part of the TEXTOR-94 program. The TEXTOR-94 tokamak provides exceptionally good access for a large variety of diagnostics. For this reason it is well suited to serving as a test-bed for new plasma diagnostics equipment. Moreover, TEXTOR-94 is mechanically very rigid and can withstand disruptions, thus allowing research on this important topic. Furthermore, TEXTOR-94 is equipped with adequate diagnostic systems for studying MHD instabilities and sawteeth. A pellet injector is installed on TEXTOR-94 that can launch 9 pellets during a discharge from the outboard as well as from the inboard side. A dynamic ergodic divertor is under construction and will be implemented on TEXTOR-94 in 2000.

The camera system will be flexible enough to be applied to various machines. After the first tests, which will be performed on TEXTOR-94, the system will be applied on the W7-AS stellarator and possibly later on other devices. As our new camera, which can work with visible as well as X-ray light, possesses great flexibility and high time resolution, there might exist a lot of new applications that we did not think of so far – not necessarily restricted to plasma physics.

7.3 Experimental Setup and Procedure

The aim of this research proposal is to develop fast, two-dimensional, tangential, soft X-ray imaging and study MHD instabilities and magnetic islands in magnetic fusion plasmas. For this purpose a soft X-ray pinhole camera which views the plasma tangentially and obtains two-dimensional pictures with a spatial resolution of 100×100 pixels and a framing rate of 100 kHz or more is planned. At present these framing rates can be achieved only for a pre- or post-triggered sequence of 32 pictures. However, in the future a sequence of 300 pictures is envisaged. In our camera the X-ray image created by the pinhole is converted to a visible image by a scintillator screen. The visible image is then recorded by a special fast framing CCD camera that employs on-chip storage. The pictures give information about the plasma X-ray emission in space and time. Since the X-ray emission can be

assumed to be constant on a magnetic surface, the images also relate to the structure of the magnetic field in the plasma. These pictures can be supplemented by other diagnostics to incorporate data of density, electron temperature, and magnetic field. The experimental data obtained in this way can be compared with the predictions of different existing MHD plasma theories and used to assess their validity.

The camera system will consist of a pinhole camera with a pinhole of variable size in the 1...3 mm diameter range, a thin beryllium window which is transparent above 800 eV, and a fluorescent plate 10 cm in diameter to convert the X-ray image to the visible spectrum. This part of the system is in vacuum.

Adjacent to the fluorescent plate there is a 2 m long optical fibre bundle with 15,000 fibres 0.75 mm in diameter. This fibe ebundle serves to guide the light far enough away from the strong magnetic field of the main field coils, where it can be amplified by a Hamamatsu V4440 electron beam based light amplifier. The transmission of the system yields about 1 electron from the photocathode of the image amplifier per X-ray quantum at the fluorescent plate. The image amplifier reduces the size of the picture to a diameter of 2.5 cm.

The endplate of the light amplifier is imaged with an optical lens onto a fast framing CCD camera with on-chip storage. The data are finally stored in a computer system for further processing.

The data obtained in this way give the emission along a line of sight, i.e. a sinogram of that emission or the Radon transform of it. To obtain local emission data, it is necessary to invert the Radon transform and obtain a tomogram. In the field interpreting the experimental results, we can refer to the published work, for example, we have developed models for disruptions and the sawtooth crash which we would like to test.

7.4 Diagnostic and Scientific Goals

The fast soft X-ray camera system is an instrument with novel features, and our effort and time will be allocated to three tasks: (1) installation and optimization of the camera hardware, (2) development of the data acquisition and data analysis software, and (3) use of the instrument as a research tool to study MHD instabilities and other plasma phenomena. The last point is of course the one that really interests and motivates us.

7.4.1 Camera installation and optimization

After completion and preliminary testing of the camera in the laboratory, the instrument will be installed on our large plasma machine, the TEXTOR tokamak, and tested there under real-life conditions for the first time. It is important to note that the TEXTOR machine, on which the camera will be tested, provides first of all a plasma of sufficient size and with sufficiently high temperature to supply a flux of soft X-rays that is large enough to allow measurements with sufficient space and time resolution. Another requirement is that the test-bed provides easy access to the machine and flexibility in the experimental programme. TEXTOR meets these conditions. There is good viewing access because the machine possesses oversized toroidal field coils and TEXTOR's experimental programme,

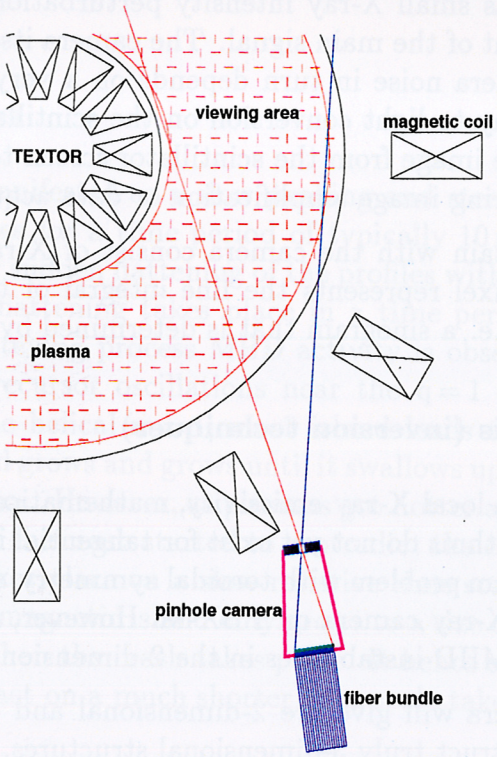

Figure 25: A pinhole camera viewing the TEXTOR plasma in the toroidal direction. The soft X-rays are converted to visible light on a fluorescent plate. The light is guided out of the strong magnetic field of the main field coils by a fibre optic cable into an image amplifier. This part is depicted in fig. 26. The picture obtained in this way is a sinogram of the luminosity integrated along the lines of sight. We can make use of the helical structure of the tokamak plasma for the inversion.

containing such features as sawtooth research, MARFE studies, and RI mode confinement, provides plasmas with rather high energy content. This general research programme and also the dynamic ergodic divertor programme supply a large variety of target plasmas that allow the camera system to be tested over a broad range of plasma parameters.

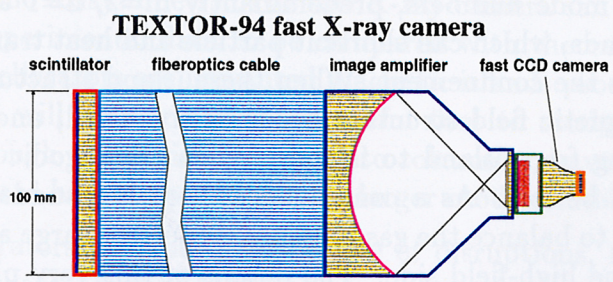

Figure 26: The part of the camera consisting of a fluorescent plate (left), a fibre bundle, a Hamamatsu V4440 image amplifier, and a fast CCD camera with on-chip storage. (see fig. 25 for the arrangement on TEXTOR).

The following problems need to be solved. MHD fluctuations and magnetic islands show up on X-ray images as small X-ray intensity perturbations which aare typically in the range of 1 to 5 per cent of the main signal. The camera itself has, therefore, to have very small noise. The camera noise in turn depends on a very large number of factors, e.g. the uniformity of X-ray to light conversion on the scintillator screen, or noise picked up in the transport of the image from the scintillator screen to the image converter tube, or processes occuring during image amplification or data acquisition by the CCD camera.

The data that we obtain with the camera consist of X-ray images where the intensity recorded with each pixel represents the line integral of the plasma soft-Xray emission along a line of sight, i.e. a sinogram that is determined by the pinhole camera geometry.

7.4.2 Data analysis (inversion techniques)

In order to obtain the local X-ray emissivity, mathematical inversion algorithms have to be applied. The algorithms do not yet exist for tangential imaging and have to be worked out. For the equilibrium problem with toroidal symmetry, some inversion codes have been written for the hard X-ray camera on PBX-M. However, nothing has been done, to our knowledge, to invert MHD instabilities in the 2-dimensional tangential view.

The images the camera will give are 2-dimensional and they do not contain sufficient information to reconstruct truly 3-dimensional structures. However, we can assume that since the X-ray luminosity depends on the electron temperature and plasma density and since these two are constant along the magnetic lines of force, the emission has a helical structure. This imposed helical structure is a constraint which reduces the problem of inversion to one of two,dimensions. We envisage proceeding along a similar line [34].

7.4.3 Disruption investigations

Disruptions in tokamaks are accompanied by a sudden quench of the plasma current which in turn produces currents in the vacuum vessel and imposes large forces on the components of the machine. These forces become very strong when the current is large, i.e. they represent a real threat to large machines, in particular a thermonuclear reactor. For this reason, disruptions should be avoided. The cause of ost of the disruptions are MHD instabilities with low mode numbers, predominantly m=2, n=1 and m=3, n=1. They produce magnetic islands, which can shortcut particle and heat transport, an undesirable effect because it spoils the confinement. When these island structures grow so large that they overlap, the magnetic field structure becomes ergodized, and the plasma particles can escape by jumping from island to island. When the ergodic structure touches the walls, the plasma will be lost. As a consequence there is a sudden pressure drop. The vertical magnetic field to balance the gas pressure is then too large and pushes the remaining plasma towards the high-field side. The details of this very plausible, but complex, theoretical sequence of events need to be verified. In particular, it was found on TFTR and other large tokamaks that there exists a terminal phase during which most of the quenching of the plasma current occurs. No proper explanation for this phase in terms of MHD instabilities is at hand.

The fast imaging system can serve to get detailed pictures of the different stages of the

disruption process, from the onset of island formation to the ergodization and the current quench.

7.4.4 Sawteeth instabilities

The sawtooth phenomenonismanifested as a slow peaking and steepening of the plasma density and temperature profiles for a time period of typically 10 ms to several 100 ms, which is then followed by a very sudden flattening of the profiles within the $q = 1$ magnetic surface of the tokamak. The flattening takes place in a time period of approximately 300 μs. At the start of the flattening process MHD activity is observed which has been identified as a $m = 1$, $n = 1$ precursor oscillations near the $q = 1$ surface. It was first believed that the growth of the helical $m = 1$, $n = 1$ island leads to complete magnetic reconnection, whereby the island grows and grows until it swallows up the complete plasma region interior to the $q = 1$ surface. However, as plasmas got hotter and their conductivity increased the short time scale of the crash started to contradict the complete reconnection or Kadomtsev model, which takes place on a slow resistive time scale. Investigations on TEXTOR have shown that the magnetic island only grows to a size of approx. 20% of the diameter of the $q = 1$ surface, when the crash takes place. It hence seems very likely that other physical processes which act on a much shorter time scale take over at the moment of the crash.

Several theories have been put forward to explain the crash event. These theories are contradictory and more experimental evidence is needed to provide a correct answer. With the fast camera system we hope to get detailed pictures during the different stages of the sawtoothing process from which we can infer the flow patterns involved. In this respect it is of particular interest whether they are monopole as it is suggested by theories which predict strong overall transport enhancement either due to ergodization or due to plasma fluctuations, or whether they are rather dipole-like, which is favoured by theories based on extension of the Kadomtev model by implementing additional terms.

7.4.5 Stellarator applications

The magnetic configuration of stellarators is more complicated than that of tokamaks. This is because there is no axisymmetry. The soft X-ray camera can depict magnetic flux surfaces and provide experimental data to be compared with theoretical predictions. Of particular concern to stellarators are unwanted magnetic islands produced by field errors. The soft X-ray camera will furthermore be a useful tool to study island divertors on stellerators, which although topologically similar to tokamaks, have a more complicated structure because they are helical and do involve larger mode numbers.

Finally, although stellarators are known to be free of disruptions, there is still a lot of MHD activity left in stellarators, e.g. GAE modes, and the fast camera is a welcome tool for its investigation.

7.4.6 Pellets

To fuel fusion devices not just from the boundary, pellets are used. These pellets have speeds of the order of km/s. There are a number of open physics questions concerning pellet injection. Ablation of the pellet due to heating by the plasma is not fully understood. Although theories about this ablation do exist one cannot be sure whether or not they are correct in all details, unless they are confirmed by experimental observations.

In particular, striations have been observed to be associated with pellet ablation. It is not clear what the striations are due to, whether the cold pellet plasma simply expands along magnetic field lines or whether instabilities develop during the pellet ablation which release gas clouds in a more pulsed manner.

The pellet can cause MHD instabilities on its way across the plasma. We see examples of this on TEXTOR as well. These MHD instabilities will show up on an X-ray picture through the cold islands they create.

7.4.7 Other applications

Other applications in the visible range of the spectrum are MARFEs and the dynamic ergodic divertor. The latter will be installed on TEXTOR-94 in the near future. It will produce very complex magnetic structures in the plasma. With plasma even the stationary structure may differ from theoretical predictions because the currents in the ergodic layer can give rise to changes in the magnetic flow pattern. When the ergodization field is being rotated it in parts a torque to the plasma.

The dynamic ergodic divertor is the subject of an application for funding and the physics aspects are discussed therein. The fast framing camera will be a very valuable diagnostic tool providing information on the magnetic structures during operation. The X-ray images will tell how far the ergodization field has penetrated and to what degree the rotation of the plasma follows that of the divertor magnetic field. As in the case of the MARFEs, one will probably want to view the boundary zone in different spectral ranges as well. Measurements in the soft X-ray range will tell how the plasma core is affected.

Because of both, the good space and time resolution, there might be a lot of applications in both plasma physics and other fields, e.g. synchrotron radiation or fast flows of fluids or gases, and there might be applications we have not thought of so far.

7.4.8 Conclusions

Owing to the combination of good time and space resolution, the fast 2-D camera system is going to provide experimental evidence which cannot be obtained by any other diagnostics. The system will be very flexible and will be used on different types of machines such as tokamaks and stellerators. For this reason it has the capability of clarifying a number of open questions in the field of nuclear fusion.

References

[1] BURRELL, K. H. et al., Phys. Plasmas **4** (1997) 1499.

[2] SYNAKOWSKI, E. et al., Plasma Phys. Controlled Fusion **40** (1998) 581.

[3] MOREAU, D. et al., 16th IAEA Conference on Fusion Energy, 1998, Yokohama/Japan, paper IAEA-CN-69/CD2/EX9/1.

[4] WOLF, R. C. et al., Advanced tokamak operation on ASDEX Upgrade, in *Plasma Physics and Controlled Nuclear Fusion Research 1998*, volume 0, pages –, Vienna, 1998, IAEA.

[5] GÜNTER, S. et al., Nucl. Fusion **38** (1998) 325.

[6] BHATNAGAR, V. et al., Nucl. Fusion **34** (1994) 1579.

[7] PETTY, C. et al., Fast wave current drive in diii-d, in *Plasma Physics and Control. Nucl. Fusion Research, (15th. Int. Conf., Seville, 1994)*, page 211, IAEA.

[8] PETTY, C. et al., Fast wave current drive in diii-d, in *Plasma Physics and Control. Nucl. Fusion Research, (15th. Int. Conf., Seville, 1994)*, page 211, IAEA, 1994.

[9] FOREST, C. et al., Phys. Plasmas **3** (1996) 2846.

[10] WILSON, J. et al., ICRF in D-T plasmas in TFTR, in *Radio frequency Power in Plasmas, (11th Top. Conf., Palm Springs, CA, 1995)*, page 3, AIP, 1996.

[11] SAOUTIC, B. et al., ppcf **36** (1994) B123.

[12] MAJESKI, R. et al., Phys. Rev. Lett. **76** (1996) 764.

[13] Becoulet A. and European Coordinating Committee, pers. com.

[14] EHST, D. et al., Nucl. Fusion **31** (1991) 1933.

[15] BÉCOULET, A., Plasma Phys. Controlled Fusion **38** (1996) A1.

[16] NOTERDAEME, J.-M. et al., Variation of the sawtooth activity with ICRF in ASDEX Upgrade, in *Europhysics Conference Abstracts (Proc. of the 2nd Europhysics Topical Conference on Radio Frequency Heating and Current Drive of Fusion Devices, Brussels, 1998)*, edited by JACQUINOT, J. et al., volume 22A, pages 9–12, EPS, 1998.

[17] NOTERDAEME, J.-M. et al., ICRF heating results in ASDEX Upgrade and W7-AS, in *Plasma Physics and Controlled Nuclear Fusion Research 1996*, volume 3, pages 335–342, Vienna, 1997, IAEA.

[18] NOTERDAEME, J.-M. et al., editors, *Proceedings of the IAEA TCM on Ion Cyclotron Resonance Heating / Edge Physics*, Elsevier, 1990.

[19] NOTERDAEME, J.-M. et al., ppcf **35** (1993) 1481.

[20] LACKNER, K., Comments Plasma Phys. Controlled Fusion **13** (1990) 163.

[21] RYTER, F. et al., Dimensionally similar studies of confinement and H-mode transition in ASDEX Upgrade and JET, in *Plasma Physics and Controlled Nuclear Fusion Research 1998*, volume 0, pages –, Vienna, 1998, IAEA.

[22] Technical basis for the ITER final design report, cost review and safety analysis (FDR), 1998, ITER EDA Documentation Series No. 16.

[23] SCHNEIDER, R. et al., J. Nucl. Mater. **266–269** (1999) 175.

[24] KAUFMANN, M. et al., Energy and particle control characteristics of the ASDEX Upgrade "LYRA" divertor, in *Plasma Physics and Controlled Nuclear Fusion Research 1998*, volume 0, pages –, Vienna, 1998, IAEA.

[25] ITER physics basis, 1998, to be published in Nucl. Fus.

[26] GREENWALD, M. et al., Nucl. Fusion **28** (1988) 2199.

[27] TAKASE, Y. et al., High power density H-Modes in Alcator C-Mod, in *Plasma Physics and Controlled Nuclear Fusion Research 1996*, volume 1, page 475, Vienna, 1997, IAEA.

[28] SCHNEIDER, R. et al., Test of the predictive capability of B2-EIRENE on ASDEX Upgade, in *Plasma Physics and Controlled Nuclear Fusion Research 1998*, volume 0, pages –, Vienna, 1998, IAEA.

[29] BOSCH, H.-S. et al., Extension of the ASDEX Upgrade programme: Divertor II and tungsten target plate experiment, Technical Report 1/281a, IPP, Garching, Germany, 1994.

[30] FINKEN, K. H., Fusion Engineering and Design **37** (1997) 335.

[31] LICHENBERG, J. A. et al., editors, *Regular and Stochastic Motion*, Applied Mathematical Sciences38, Springer, 1983.

[32] ABDULLAEV, S. S. et al., Physics of Plasmas **5** (1998) 196.

[33] FINKEN, K. H. et al., Nucl. Fusion **38** (1998) 515.

[34] FUCHS, G. et al., Plasma Phys. Controlled Fusion **40** (1998) 91.